Fall 2017

Doppler LiDAR Measurements of Boundary Layer Heights Over San Jose, California

Matthew Robert Lloyd
San Jose State University

DOPPLER LIDAR MEASUREMENTS OF BOUNDARY LAYER HEIGHTS OVER SAN JOSE, CALIFORNIA

A Thesis

Presented to

The Faculty of the Department of Meteorology and Climate Science

San José State University

In Partial Fulfillment

of the Requirements for the Degree

Master of Science

by

Matthew R. Lloyd

December 2017

The Designated Thesis Committee Approves the Thesis Titled

DOPPLER LIDAR MEASUREMENTS OF BOUNDARY LAYER HEIGHTS OVER SAN JOSE, CALIFORNIA

by

Matthew R. Lloyd

APPROVED FOR THE DEPARTMENT OF METEOROLOGY AND CLIMATE SCIENCE

SAN JOSÉ STATE UNIVERSITY

December 2017

Dr. Craig Clements	Department of Meteorology and Climate Science
Dr. Martin Leach	Department of Meteorology and Climate Science
Dr. Neil Lareau	Department of Meteorology and Climate Science

ABSTRACT

DOPPLER LIDAR MEASUREMENTS OF BOUNDARY LAYER HEIGHTS OVER SAN JOSE, CALIFORNIA

by Matthew R. Lloyd

There is a need for understanding boundary layer depth and climatology over the urban area of San Jose, California. In this paper, Doppler LiDAR data are observed from San Jose. The adopted methods of vertical velocity variance and skewness are used to determine the estimated height of the convective boundary layer and to analyze sources of turbulence. The use of these methods helped identify a few types of the boundary layer that are common in San Jose. Also examined in this paper is a brief climatology of the mean maximum convective boundary layer height in San Jose over the period of 2013-2015. Vertical velocity variance and skewness is applied to identify seasonal trends in the convective boundary layer height. The influence that the marine layer has on the boundary layer over San Jose is analyzed and a conduit for future work is set forth.

ACKNOWLEDGMENTS

The completion of this SJSU Master's Thesis is due to the efforts of many individuals. First, thanks to my advisor, Dr. Craig Clements, for initiating my involvement with one of his research opportunities that ultimately led to the creation of this Master's Thesis. Dr. Clements' support greatly impacted the success of this Master's Thesis. I also thank Dr. Martin Leach for the assistance and feedback that was provided. His input and advice is incredibly appreciated. Special attention and thanks are noted to the efforts of Dr. Neil Lareau; his help was irreplaceable. Dr. Lareau's assistance and guidance with the data, mentoring with the computer programming scripts, and direction throughout much of the Master's Thesis planning was a core to its success.

Many thanks are due to my family, friends, and professors within the SJSU program for their help and support in this endeavor. Lastly, the support of my wife, Katie, was key to the timely completion of this Master's Thesis. She sacrificed many hours, days, and months, and encouraged me to persist and accomplish this final task to qualify for the Master's Degree. She helped me pursue my hobby, passion, and future career in meteorology.

TABLE OF CONTENTS

LIST OF FIGURES

1. Introduction

The fields of air quality, atmospheric pollution dispersion, and wind energy can all benefit from a greater understanding of the dynamics of the planetary boundary layer (PBL). The depth or height of the PBL is a fundamental parameter for any boundary-layer study or model, either physical or chemical (Angevine et al. 1994). Numerous PBL studies have implemented active remote sensors such as wind profilers, microwave profilers, Sonic Detection and Ranging (SoDAR) or high-resolution Doppler Light Detection and Ranging (LiDAR) as tools to observe and analyze the structure of the PBL. These studies define the height of the PBL differently. For example, one Doppler LiDAR technique uses idealized backscatter profiles (Steyn et al. 1999), in which the backscatter ratio is produced as a robust method for an automated detection scheme. Another technique for estimating the height of the PBL is by Eresmaa et al. (2012), in which ceilometer data are utilized. The three-step idealized-profile method utilizes backscatter to identify the sub-layers in the PBL. An older technique by Angevine et al. (1994) use a 915 MHz boundary layer profiler. This involves the procedure of a signal-to-noise ratio (SNR) that is recorded by the profiler; a peak in the range-corrected SNR indicates the top of the PBL (Angevine et al. 1994).

Cohn and Angevine (2000) use two Doppler LiDAR units and a radar wind profiler to analyze the measurements of the boundary layer and entrainment zone thickness. The aerosol content within the PBL is proportional to the backscatter observed by the Doppler LiDAR. In the study, the moisture gradients and turbulence strength are the key parameters for the radar wind profiler backscatter to identify the height of the PBL. A

wavelet transform technique is used to correlate the results between the wind profiler and Doppler LiDAR.

A more recent study applies the approach of vertical velocity variance (σ_w^2) by Tucker et al. (2009) and a focus on vertical velocity skewness (SK) by Hogan et al. (2009). The height of the mixed layer within the PBL is identified using the σ_w^2 method. Variance of vertical velocity will help determine areas of the PBL that are more turbulent. Where this diminishes rapidly, approaching zero, can be an estimation of the height (or upper bound) of the mixed layer. The SK method aids in identifying the sources of turbulence within the PBL. The σ_w^2 and SK methods are described further in Chapter 3.

2. Boundary Layer

In this chapter, the PBL anatomy, application of PBL meteorology, and three common types of the PBL in San Jose are discussed.

a. Background on Boundary Layer Meteorology

The PBL comprises the lowest layers of the troposphere. It is directly influenced by the surface of the earth and responds to surface forcing with a time scale of one hour or less (Stull 1988; Hägeli et al. 2000). This surface forcing drives the diurnal growth and decay of the convective boundary layer (CBL), except for times of synoptic disturbances. Therefore, the CBL is frequently analogous to the daytime PBL, in which the PBL represents the boundary layer at any given time, whether day or night.

The height of the CBL varies in response to upwelling buoyant parcels of air from insolation at the surface and the compensating down-welling parcels of air from above

(Eichinger et al. 2005). This insolation is partitioned into sensible, latent, and ground heat fluxes. The sensible and latent fluxes cause positively buoyant parcels to form and drive the vertical development of the CBL. The CBL is a region of frequent and highly turbulent motions leading to well-mixed profiles of potential temperature and water vapor mixing ratio. These eddies vary in magnitude in both time and space. The largest eddies scale with the depth of the CBL itself. With respect to the CBL height, small but intense eddies are typical during a growing CBL in the morning and throughout the afternoon during cloudless or cumulus-topped PBLs (Hogan et al. 2009). On the contrary is the production of large, weak eddies that envelop most of the decaying PBL during the nighttime or particularly in the case of a cloud-topped PBL. The nocturnal PBL begins as the surface heat flux becomes negative, which typically occurs near sunset. The CBL height subsequently decays, leaving a wake of residual turbulence, or weaker eddies, known as the residual layer (RL).

The extent and timing of CBL growth is dependent upon, or influenced by, many meteorological and geographical factors including: land-surface characteristics (e.g., irrigation patterns), synoptic-scale subsidence, synoptic horizontal wind convergence or divergence, mesoscale motions such as upslope and downslope flows driven by topography, sea and land breezes, solar radiation, precipitation, and patterns of differential temperature advection (Bianco et al. 2011). The structure of the PBL is fluid, and is continually molded by these factors. The idealized concept of the CBL growth is often not observed in nature due to these real world complexities. Some of these elements are analyzed in Chapter 4.

During synoptically quiescent periods, the CBL height generally follows a common, even predictable, diurnal pattern. Initial CBL height growth can typically be observed shortly after sunrise because of the influence of surface sensible heat flux (*H*). The CBL height typically peaks in the early to mid-afternoon and decays in the late afternoon as *H* diminishes. Once the sun sets, the CBL has collapsed. The rate of growth of the CBL height can be measured by the rate at which energy is introduced into the PBL (Eichinger et al. 2005). The daily evolution of the CBL consists of entrainment fluxes from aloft (Stull 1988) and *H*. These are key elements to the growth rate and potential height of the CBL.

Figure 1 shows a general interpretation of the PBL evolution throughout the day. The CBL is typically divided into three main layers: the surface layer (SL), mixed layer (ML), and entrainment zone (EZ). Figure 1 is modified from Stull (1988).

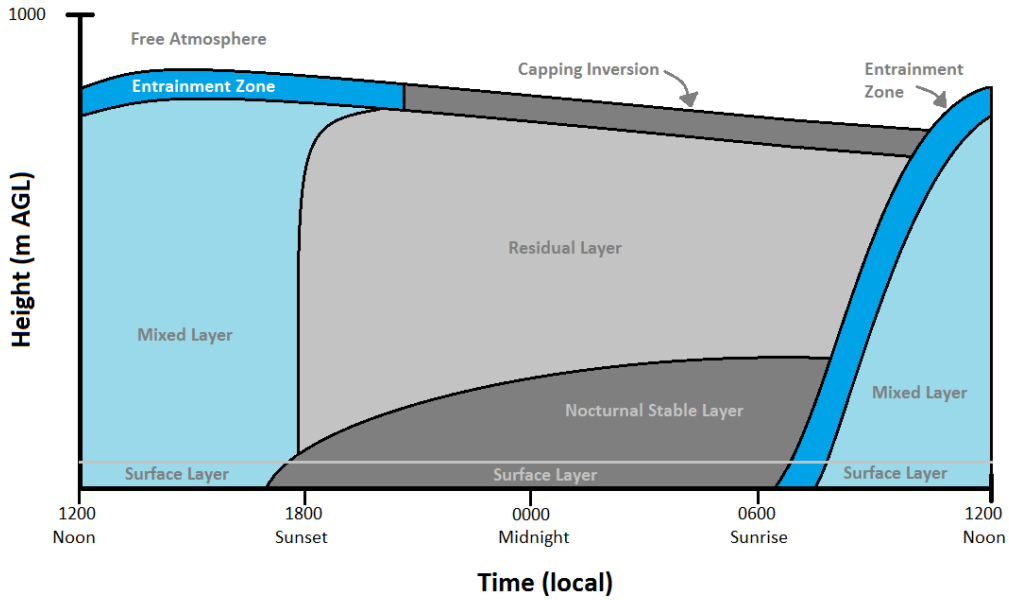

Figure 1: The anatomy of the PBL over a land surface during high pressure conditions.

The SL, typically the lowest 50-100 m of the boundary layer, is where the highest gradients in wind speed, temperature, and humidity occur (Kaimal and Finnigan 1994). Within the SL, the turbulent exchange of heat, mass, and momentum is highest, greatly impacting the entire PBL (Kaimal and Finnigan 1994). The winds within the SL are not affected by largescale winds, but primarily by surface friction and the vertical gradient of temperature (Kaimal and Finnigan 1994).

The region above the SL, and extending up to the base of the EZ, is the ML. This is the deepest layer in the PBL. Similar to the SL, the ML is impacted by surface friction and the temperature gradient. It is also known that over a homogeneous surface, turbulent mixing and heat transfer within the ML is predominantly vertical (Wang and Bras 1998).

The uppermost layer within the PBL is the EZ, which separates the ML and the free atmosphere (FA). For the purpose of this paper, the height of the EZ is analogous to the estimated CBL height and is further discussed and analyzed in the case study in Chapter 4. The EZ is the permeable interface between the ML and the FA in which entrainment of free tropospheric air takes place. The typically warmer, dryer air aloft mixes downward and assists in the warming of the ML, forming a discontinuity in the vertical gradients of potential temperature and humidity profiles (e.g. Cleugh and Grimmond 2001). The perturbations in the potential temperature and humidity profiles assist in identifying the transition from the ML to the EZ, or in essence, the upper bound of the CBL.

Heat, moisture, and aerosol from the surface of the earth is first mixed through the PBL before becoming available to the circulation of the FA (Hägeli et al. 2000). The interface between the FA and PBL (namely the EZ) is normally strongly convoluted

(Hooper and Eloranta 1986). Doppler LiDAR data may be used to analyze the returns of aerosol backscatter to identify the approximate boundary between the PBL and the FA.

The winds within the FA are primarily impacted by larger mesoscale and synoptic scale conditions. The FA is also distinguished from the layers within the PBL because it is not directly influenced by surface friction. It is also typically less polluted by particulates or aerosols in the FA than within the PBL. The FA has fewer variations in backscatter (Eresmaa et al. 2012) and is not as detectable by Doppler LiDAR and other remote sensing instrumentation.

As the sun sets, the influence of *H* is reversed. This results in the collapse of the turbulent and remnant CBL becoming the RL during the night (Figure 1). In conjunction with the collapse of the CBL, turbulent eddies within the CBL become slower (both temporally and spatially). As discussed later in Chapter 3, the SK of the vertical profile at this time would be expected to become more neutral or negative (under conditions absent of local, low-lying cloud bases) because the predominant source of daytime surface-based turbulence is shut off. If there are no large-scale synoptic influences, the RL is typically present between sunset and sunrise as a region of decreased residual turbulence. This can be identified from Doppler LiDAR data. Where there is weak σ_w^2, yet residually high aerosol backscatter during nighttime, it can be estimated that the RL is present.

The PBL is ever-evolving due to the external forces described. While the PBL profile and the CBL height growth is not always predictable or understood, the methods and techniques in case studies in this paper demonstrate how Doppler LiDAR can be utilized to observe and analyze the various types of the PBL. Throughout this paper the usage of

"PBL" encompasses all parts of the boundary layer from the surface to the uppermost layer during the day or night. However, "CBL" refers specifically to the growth of the boundary layer during the day resulting from convection.

b. Boundary Layer Application

PBL meteorology has many applications, but is particularly important in understanding air quality and wind energy production. For example, due to the restricted mixing volume of the PBL, containment of near-surface emissions is an especially important consideration for air quality management. Entrainment and transport of these pollutants to the FA are most likely to occur during the more turbulent mixing periods, beginning with the CBL height growing phase in the morning until the strongest mixing diminishes in the afternoon. Turbulent mixing is reduced in evening hours, assuming there are no synoptic disturbances. Any synoptic disturbances influencing the region could encourage the entrainment and transport of pollutants from the PBL to the FA.

In the upper PBL is the EZ, which is especially important as a transitional zone between the PBL and FA (Hägeli et al. 2000), as the concentrations of aerosol and air pollutants are typically higher in the PBL than in the FA aloft. Being where we live and breathe, the PBL is of keen interest for air quality studies and management facilities. The state of the PBL greatly impacts the forecasts for air quality and atmospheric pollution dispersion. A PBL with a rapidly growing CBL, or sufficient vertical mixing, would likely contribute to the entrainment of gases, pollutants and particles from the PBL to the FA and vice versa. Knowing the estimated CBL height is a significant parameter to

determine the volume of pollution transport and dispersion (Wang et al. 2012) and to forecast pollution concentrations.

Terrain-enhanced flows can impact the transport of air in the lower troposphere. The timing of CBL growth and decay are also necessary to aid in the estimation of the near-surface pollution concentration or the entrainment of pollutants into the FA. Reuten et al. (2005) states that air pollution in the PBL is often altered by slope flows due to elevated terrain. This plays an important role in the exchange of air masses known as handover processes (Ketterer et al. 2014; Kossmann et al. 1998). Cloud and mountain venting assist in the mixing of air within the PBL (Ketterer et al. 2014).

The dynamics of the PBL are also important for wind energy applications. Doppler LiDAR scans can be useful for applications such as studies on the turbulent wake eddies from wind turbines [e.g. Rhodes and Lundquist (2013)]. Doppler LiDAR is an instrument that is suitable for obtaining high temporal and spatial resolution. Identifying the mean and turbulent structure of the CBL with high temporal and spatial resolution is important for optimal operation of wind farms (Frehlich 2008). Rapid changes in wind velocity, or turbulent motions, can greatly influence the power production of a wind farm and affect maintenance issues such as excessive loading and vibration (Frehlich 2008).

BL conditions may greatly impact the safety of transportation. For instance, a coastal region or a saturated PBL may often experience foggy conditions creating poor visibility. This is a hazard to various modes of transportation that may produce a risk to the safety of the transportation of people and cargo. Those impacted could include air travel, boats, road vehicles, and others.

Future research of climate change's effects on the PBL could be of interest. Climate change may gradually impact the climatology of the Earth's PBL. Changes in insolation of the earth's surface due to altered cloud cover may enhance or suppress the amount of mixing or growth of the CBL height or other wind parameters. Changes in temperature, downward solar radiation (due in part to changes in cloud cover), precipitation frequency, stagnation events, and ventilation could affect air quality in several regions (Leung and Gustafson 2005). Understanding and predicting the PBL can be difficult across diverse climates and topographic regions, yet it plays an essential role for meteorological and climatological applications. The impacts that climate change may have on the PBL would affect everyone, either directly or indirectly.

c. Common Boundary Layer Types

The PBL can be categorized by distinct physical characteristics. These include both the cloud-topped and cloudless PBL. While the PBL (particularly the CBL within the PBL) is ever evolving, these characterizations are generalized to best identify the mechanics and apply the methods utilized in Chapter 3.

The cloud-topped boundary layer includes two main types: the fair weather cumulus-topped PBL that consists of more buoyant and unstable conditions, and the marine-influenced stratocumulus-topped PBL. While both of these are capped with a temperature inversion, they are distinguished from one another by their source of turbulence. The source of turbulence in the fair weather PBL is predominantly from the surface, while the marine-influenced stratocumulus-topped PBL can experience turbulence sources within the cloud layer. These two cloud-topped PBLs are quite different in their composition.

The skewness of the vertical velocity is one mode to identify these differences and classify the PBL in various atmospheric conditions. The calculation of SK, as described in Chapter 3, allows the source of turbulence to be identified by its location and sign in the PBL profile.

The turbulence in the stratocumulus-topped PBL is driven by long-wave radiative cooling aloft and cloud top evaporative cooling (Hogan et al. 2009) rather than insolation and *H*. This is in contrast to the cumulus-topped PBL that is driven by *H*. An example is described in further detail in the case study in Chapter 4.

A cloudless PBL is driven by *H*, as is the fair weather cumulus-topped PBL, and is indicated by positive SK near the surface (Hogan et al. 2009). The upwelling of air parcels can expect narrow and intense upward motions, with weaker down-welling (Hogan et al. 2009) that is distributed over a larger region of narrow updrafts and broad downdrafts. Examples of some of the common types of the PBL are shown in this paper.

Doppler LiDAR observations are taken in San Jose, in the South San Francisco Bay (see Figure 2). When synoptic conditions permit, the cloudless PBL environment can be favorable in San Jose. Examples of this PBL type are evident in the case study in Chapter 4, in connection with a thermal low (or inverted pressure trough) that results in a changing PBL day to day.

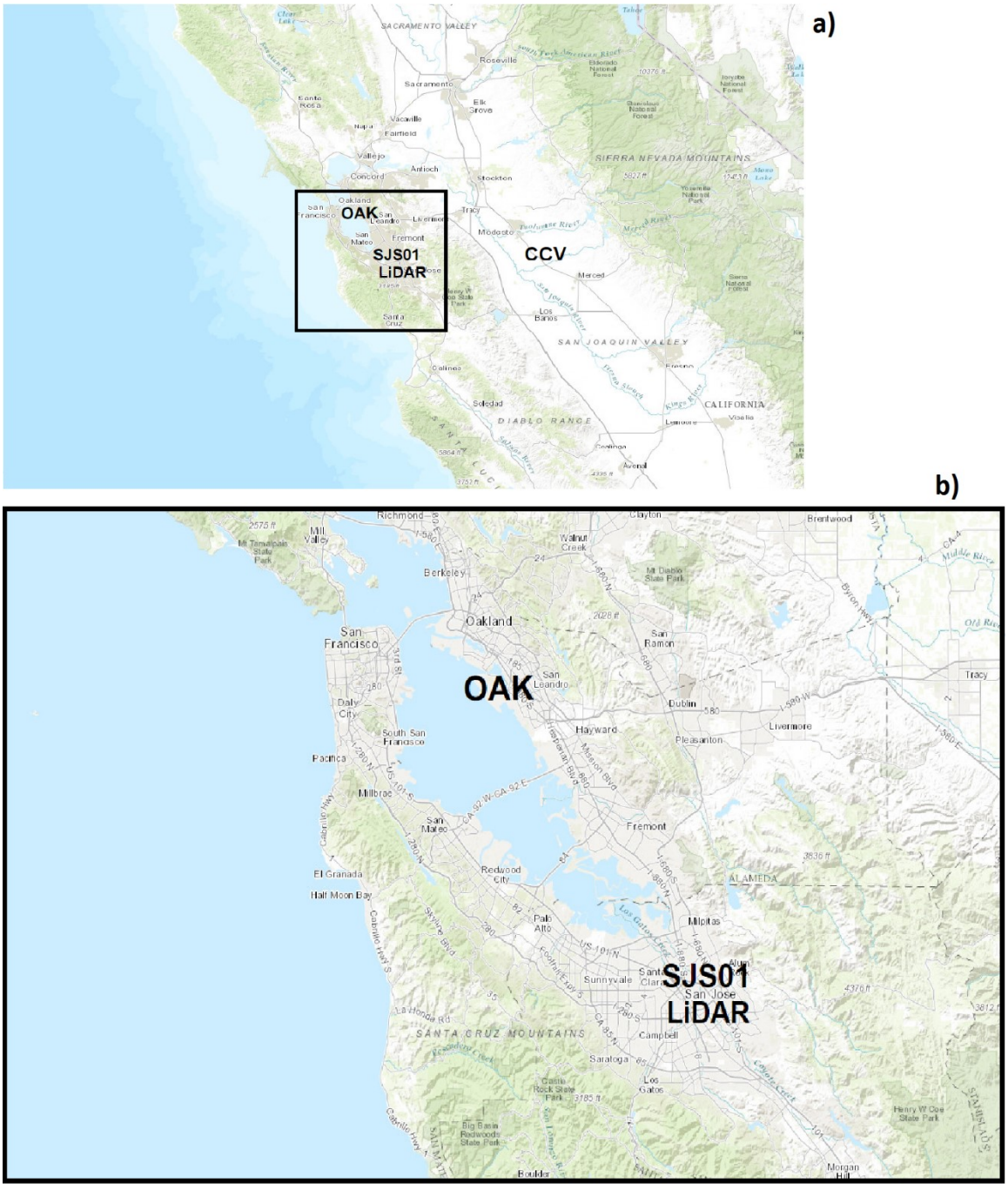

Figure 2: Domain of study in west-central California. California Central Valley (CCV), SJSU sited Doppler LiDAR (LiDAR) data (see Figures 8-19 and Figures 21-38), surface weather observation station (SJS01) (see Figure 6) at SJSU and atmospheric soundings (see Figure 4) from Oakland, California (OAK).

The composition of the PBL depends on synoptic and local atmospheric conditions. Clouds impact the anatomy of the PBL. A stratocumulus-topped PBL often forms over cool ocean currents (Moyer and Young 1991), including in San Jose. Due to the added turbulence of the cloud layer over regions such as San Jose, not only is the PBL being influenced by surface buoyancy flux, but modeling becomes more difficult and complex (Moyer and Young 1991; Nicholls and LeMone 1980). Identifying the mechanics of the PBL is discussed in further detail in the following chapter, in which methods stemming from vertical velocity are used.

With its proximity to the relatively cold Pacific Ocean, as discussed earlier, San Jose frequently experiences clear-sky CBLs and the stratocumulus-topped PBL. The stratocumulus conditions are commonly defined as a marine-influenced boundary layer (MBL). This may, at times, replace the existing surface-based CBL (McElroy and Smith 1991). While a MBL does not always present a stratocumulus layer, its influence is especially prevalent during summer months in San Jose due to increased H (from a higher solar angle and an increase in the duration of daylight). A horizontal thermal gradient is created between the land-sea-interaction that drives a summertime flow from sea to land during many summer days. An analysis of three common PBL types in San Jose is conducted in Chapter 4, including the interaction of the CBL with the MBL. There is also a short-term climatology of the PBL in San Jose in Chapter 5 that introduces the topic of seasonal PBL types in San Jose.

In the case study in Chapter 4, three specific examples of common PBL types in San Jose are identified and discussed: the clear CBL with minimal marine influence, the clear

CBL with afternoon sea breeze, and the nocturnal stratocumulus-topped PBL. The latter often extends into the early morning hours after sunrise due to the extent of marine influence.

3. Instruments and Methods

a. Doppler LiDAR and Data

In this section, the instruments (both in situ and remote sensing) and data utilized in the paper are discussed. A primary purpose of this paper is to determine the height of the daytime PBL, to examine the source(s) of turbulence within the PBL, and to analyze the characteristics of the winds within the PBL in San Jose. The approaches that are used closely follow the σ_w^2 and SK methods as key elements of analysis of the PBL for the case studies in Chapter 4. Doppler LiDAR provides high temporal resolution for the use of these two methods. The San Jose State University (SJSU) Doppler LiDAR was deployed from 2013-2015 to assist with continuing work of the California Greenhouse Gas Emissions (CALGEM) project by Lawrence Berkeley National Laboratories and affiliates with University of California (UC) Berkeley (Fischer et al., 2016). The data were collected and analyzed to correlate PBL observations with Weather Research and Forecasting (WRF) simulations.

Measuring the CBL height or wind parameters aloft can be more challenging than obtaining meteorological data at the surface. Near-surface data are found by an abundant number of in situ sensors as a part of automated weather observation stations. Other than radiosondes (that lack high temporal resolution) or the Tethered Lifting System (e.g. Frehlich et al. 2008) (requiring open spaces), the use of in situ instruments is not typically

a viable approach to physically probe the atmosphere at the heights required to reach all levels of the PBL. Remote sensing instruments such as Doppler LiDAR and SoDAR can be used for studying the PBL's characteristics, including estimating the height of the CBL, identifying areas of high turbulence, and providing high spatial and temporal resolution profiles of other wind parameters.

The Doppler LiDAR is used for atmospheric remote sensing applications such as cloud studies, wind profiling, air quality monitoring, pollution dispersion, gust monitoring, wind shear monitoring, and PBL meteorology. The Halo Photonics Stream Line pulsed Doppler LiDAR system is utilized for the data collection in this PBL study. The mode of operation of the Doppler LiDAR consists of vertical stare scans and wind profiles. The Doppler LiDAR operates with an eye-safe (Class 1M) laser in the near-infrared (IR) at a wavelength of 1.5 μm. The instrument projects the energy into the atmosphere and measures the delay in the return signal. This range- and time-resolved measurement occurs due to its sensitivity to the aerosol which is in higher abundance within the PBL than in the FA. The parameters used in this paper from the Doppler LiDAR are the following measurements: backscatter coefficient, signal-to-noise-ratio, Doppler velocity, and Doppler beam swinging for horizontal winds.

Aerosols are excellent tracers of the winds in the atmosphere, as they are often the most abundant within the ML (or CBL) of the PBL. The Doppler LiDAR retrieves and records the attenuated backscatter coefficient and Doppler velocity of the winds when aerosol is present. The range of the Doppler LiDAR is approximately 60 m to 10 km; however typical ranges are limited to 3 km or less due to atmospheric conditions and

whether there is an adequate manifestation of aerosol. The Doppler LiDAR cannot penetrate through optically thick clouds due to the high water content. Therefore, the data are generally limited to either the cloud base or the extent of the aerosol layer closest to the surface of the earth, whichever is lower in altitude. Reference to this aerosol layer will be defined throughout many of the figures as the aerosol depth (AD). The resolution of the data in this study were typically set to range gate lengths of 18 m. Data from the Doppler LiDAR were processed using 15 min averaged time intervals.

The data from the Doppler LiDAR's vertical stare scans and wind profiles were produced on top of an eight-story building at 48 m mean sea level (MSL), approximately 25 m above ground level (AGL). The location of the Doppler LiDAR was in San Jose, California, at SJSU as presented in Figure 2 at the coordinates: 37° 19.95033' N, 121° 52.91917' W.

To prevent interference, careful consideration of the Doppler LiDAR site minimized erroneous or invalid data due to nearby objects. The Doppler LiDAR uses three-field volumetric averaging to calculate wind velocities. This process is called Doppler Beam Swinging (DBS). DBS uses a mathematical retrieval method utilizing data from three beam angles in order to derive the horizontal wind velocity. First in the vertical, the Doppler LiDAR's laser determines the vertical velocity of the aerosol. At a custom azimuth angle to the north and to the east, the laser then intermittently departs from the vertical to measure the u- and v-winds.

The placement of the Doppler LiDAR on the roof allowed an unobstructed view to represent the CBL in downtown San Jose. Due to the proximity to the San Francisco Bay

that lies to the north-northwest, a common phenomenon for the area was identified in the data. Three types of the PBL in San Jose are identified in a case study. These common types of the PBL are associated with a recurring, daily sea breeze, sometimes accompanied by a sea breeze frontal passage (FROPA). The case study, including three common PBL types, is examined in detail in Chapter 4.

Other data included in this paper included the Oakland, California (OAK) atmospheric sounding profiles (about 53 km in proximity to the north of the SJSU Doppler LiDAR site) that were obtained from the University of Wyoming. Also utilized in this study are surface weather observations from the SJSU station, SJS01 (within meters of the SJSU Doppler LiDAR), obtained from MesoWest of the University of Utah (Horel et al. 2016). These sites are all represented in the study domain in Figure 2. Another dataset that is included in this paper is found in the synoptic analysis of Chapter 4. The isobaric reanalysis charts of geopotential height contours at 925 hPa are used to identify the evolution of a thermal trough over the west coast region of California and the surrounding area.

b. Methods and Techniques

Two main methods that are utilized in this paper are discussed. First is the σ_w^2 method. This is the technique used to develop the algorithm for identifying and defining the estimated CBL height using Doppler LiDAR data. Second is the SK method, which not only helps identify where the CBL is located in the daytime, but assists in determining the type of PBL and the source of turbulence (during both day and night).

1) Vertical Velocity Variance

Previous studies have utilized Doppler LiDAR data to determine the CBL height and analyze its structure. For example, the technique used by Steyn et al. (1999) utilizes backscatter data and a backscatter ratio to identify the upper bound of the ML. This paper follows the approach of Tucker et al. (2009), using the profile of the vertical velocity variance (σ_w^2), to identify the CBL top. This method is utilized in the case study in the following chapter to estimate the CBL height.

Recall that surface forcing during the day is a primary driver in the diurnal cycle of the CBL height, especially during quiescent periods that are mostly free of synoptic disturbances. The CBL is the region near the Earth's surface that is determined by surface-based turbulence (Tucker et al. 2009), whether it is dominated by *H* during the daytime, driven by long-wave radiative cooling aloft (particularly at nighttime), or cloud top evaporative cooling. The σ_w^2 profile can be determined from the Doppler LiDAR vertical velocity data to locate the maximum height of surface-based turbulence (Tucker et al. 2009). This upper bound of turbulence is analogous to the height of the CBL. Any CBL types that have other significant sources of turbulence (e.g. when there exists a low level cloud base) would benefit from other profile methods. This includes the SK method that is described in the following section in this chapter.

Eq. (1) represents σ_w^2, in which the vertical velocity variance (σ_w^2) is given by Eq. (1). In this equation, w_i is an individual observation of the vertical velocity (w), $\overline{w}$ is the time-mean vertical velocity, and n is the number of samples. Data in this paper are observed in which n equals 1 s for 15 min periods.

$$\sigma_w{}^2 = \frac{\sum_{i=1}^{n}((w_i - \overline{w})^2)}{n-1}. \quad (1)$$

A threshold is needed to identify where "significant" turbulence is present, thus defining the CBL height. Tucker et al. (2009) compared CBL height estimates from σ_w^2 profiles to the relative humidity and potential temperature radiosonde data to empirically determine a threshold value of 0.04 m^2 s^{-2} for most settings, except where a Doppler LiDAR was located on a vessel in open water, the threshold was set as 0.03 m^2 s^{-2}.

Doppler LiDAR data observed from SJSU in San Jose were used in this study. Various trials of threshold values were attempted, compared, and contrasted after being overlaid with the plotting of other parameters (e.g. aerosol backscatter, vertical velocity, and SK). These examples are described in the following section in this chapter. Following the methods from Tucker et al. (2009), the threshold of 0.1 m^2 s^{-2} was empirically determined to be the most robust for the wide time range of data that were analyzed. This threshold indicates where the sharpest gradient of turbulence and mixing occur within the CBL, or where the most rapid decrease in turbulence with increasing height is found. Recall that the estimated CBL height is this interface between the ML and the FA, or EZ, as illustrated in Figure 1.

Higher levels of σ_w^2 (0.1-1.0 m^2 s^{-2}) indicate regions of higher turbulence. This partially defines the CBL height according to this study's method of choice. However, there is a fine line between high σ_w^2 and low σ_w^2. Defining what determines high σ_w^2 versus low σ_w^2 is somewhat ambiguous. The threshold of 0.1 m^2 s^{-2} is a boundary in this study that defines what is high and low. The σ_w^2 profile is presented in Figure 3 in which the uppermost limit of the CBL, or estimated CBL height (black stars), are identified

through the period. Lower levels of σ_w^2 (0.0-0.1 m^2 s^{-2}) are indicative of lower turbulence outside of the CBL. These lower levels of σ_w^2 are often found in regions of low turbulence such as the RL, as described in Chapter 2. The σ_w^2 in Figure 3 corresponds to the timing and influence of *H* after the sun rises. CBL growth (where elevating levels of σ_w^2 are identified) begins in the morning at approximately 0700 PDT in Figure 3.

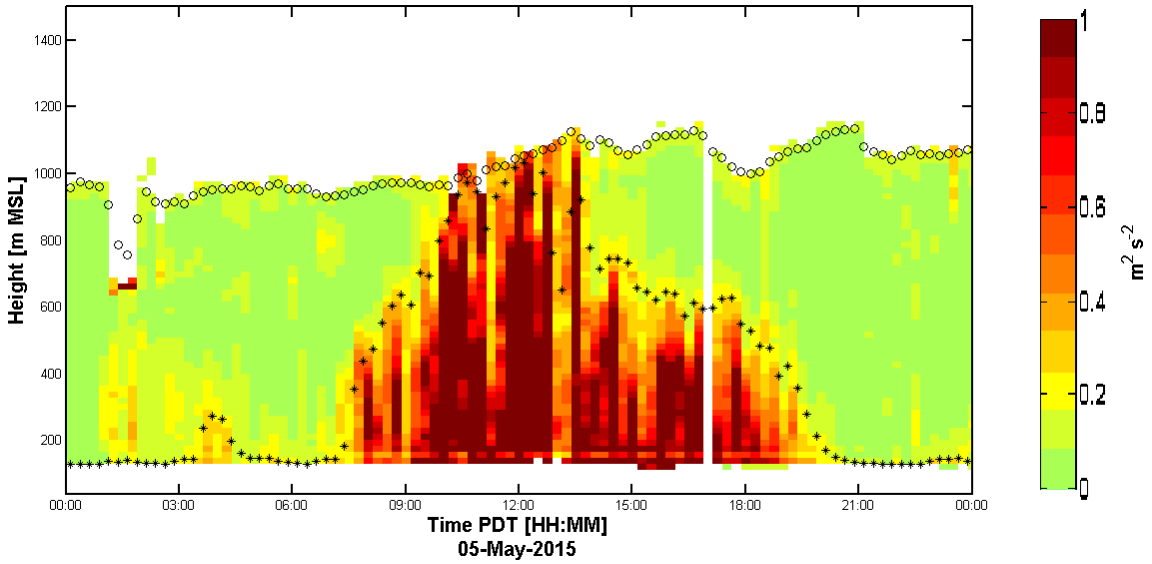

Figure 3: Vertical velocity variance derived from Doppler LiDAR at SJSU on 05 May 2015. Warmer (red and orange) colors represent a more positive vertical velocity variance (m^2 s^{-2}), while cooler (green) colors are lower values. The estimated CBL height is illustrated by an asterisk (*), and aerosol depth is illustrated by an open circle (o). The x-axis represents local time (PDT), and the y-axis depicts the height (m MSL).

Near peak *H* at midday, the CBL height reaches a maximum near 1000 m MSL (an increase of approximately 850 m in about 4.5 h). The CBL begins a gradual collapse as the afternoon wanes into evening. Preceding sunrise are some elevated levels of σ_w^2 in the lower 400-500 m of the profile. This is residual turbulence from the CBL of the previous day. This region is the RL. The upper limit of the profile is capped by the AD (open circles). This is either a result of the Doppler LiDAR's inability to identify the

aerosol at those heights or that the set threshold for aerosol is met. Note that the 18 m range gates in 15 min sampling periods were used to create the σ_w^2 and were calculated after omitting erroneous or missing data values to minimize error. During processing, the datasets that obtained more than 40% of missing data were removed.

2) Vertical Velocity Skewness

The σ_w^2 profile is helpful in identifying the PBL types described above (cloudless, cumulus-topped, and stratocumulus). PBL types are better identified using the SK profile. The σ_w^2 profile method also coincides with the SK profile to determine the estimated CBL height. This paper utilizes the Doppler LiDAR vertical stare scans to produce the SK profile for entire diurnal cycles of the PBL. The case studies in the following chapter will detail the examples of local PBL types.

Previous work by Hogan et al. (2009) suggests that the utilization of the SK profile can differentiate between types of the PBL. The cloudless and the cumulus-topped (fair weather) CBL are evident when turbulence is primarily driven by surface heating (Hogan et al. 2009). However, the nocturnal stratocumulus PBL, often analogous to a MBL structure, is represented by dominating cloud-top radiative cooling (Hogan et al. 2009). Eq. (2) adapted from Hogan et al. (2009) represents SK and is given below:

$$SK = \overline{w'^3} / \overline{w'^2}^{3/2}. \quad (2)$$

Vertical velocity (w) is utilized to determine the SK profile, in which w' is the fluctuation from the mean vertical wind (Hogan et al. 2009). The σ_w^2 is the second moment and the SK is the third moment of the vertical velocity distribution. The sign of the SK profile determines whether the turbulence is driven by surface heating or cloud-

top cooling (Hogan et al. 2009). The triple correlation $\overline{w'^3}$ represents the vertical transport of $\overline{w'^2}$ by the turbulence itself (Bougeault and André 1986; Hogan et al. 2009). The physical relevance to SK is where higher SK most commonly represent stronger, narrow updrafts and broader, weaker downdrafts.

When negative SK is manifest throughout a PBL it often represents a MBL with a stratocumulus layer. In a negative SK profile, the source of turbulence is "upside-down" in appearance in comparison to the surface-based heating found in the cloudless PBL. As buoyancy generation of turbulent kinetic energy (TKE) is at a maximum at the top of the PBL, the TKE simultaneously increases with height (Hogan et al. 2009). Down-welling motions are observed as being narrow and intense, while the upwelling air parcels are weaker (Hogan et al. 2009). Negative SK best-identifies the nocturnal stratocumulus-topped PBL. This example of negative SK is seen in the last section of Chapter 4.

When SK is positive, it can represent the cloudless or cumulus-topped PBL. This could be expected in a fair weather environment. A positive SK profile is typical during synoptic conditions where a ridge of high pressure is present. Another case of positive SK could be indicated when local low-level easterly winds (favoring continental influence) are dominant in San Jose. The turbulent transport of TKE is then upward with TKE decreasing with height. On the contrary is the negatively skewed PBL, updraghts are narrower and more intense than the weaker, broader downdraughts (Hogan et al. 2009). SK is indicative of the structure of motion, in which "bottom up" is representative of the positive SK profile, and the "top down" is the negative SK profile (Moeng and Rotunno 1990).

Figure 4 exemplifies a predominantly positive SK profile in the afternoon. See the expanse of red (positive SK) from 1200-2000 PDT. Despite some erroneous or missing data aloft during peak heating, the lower 600 m MSL to the surface represents the "bottom up" profile. It is likely that a clear CBL exists during the positive SK phase of the profile.

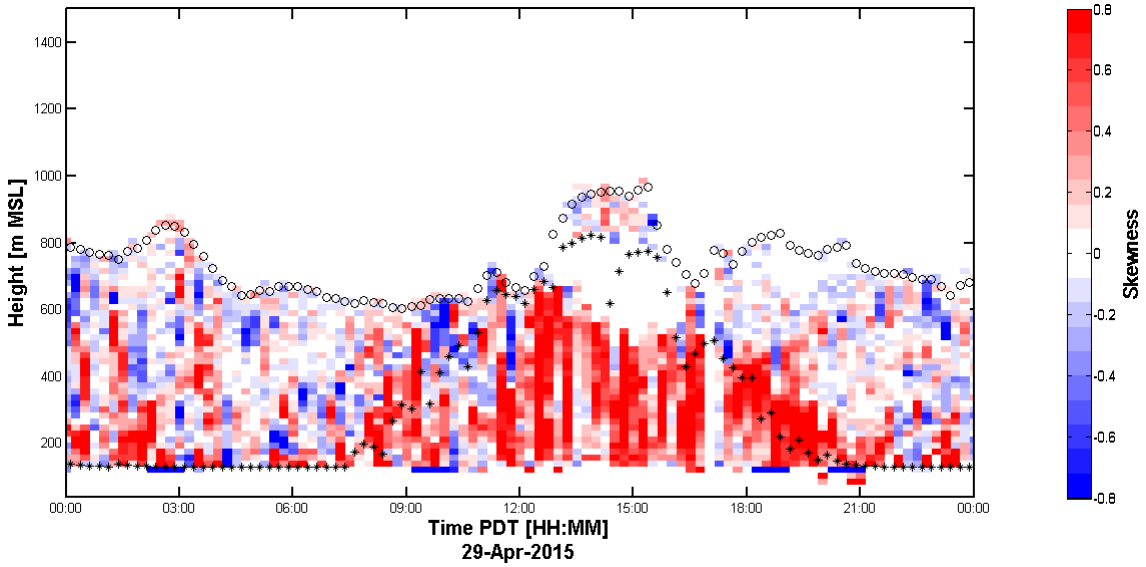

Figure 4: Vertical velocity skewness profile using Doppler LiDAR at SJSU on 29 April 2015. Warmer (red) colors represent positive vertical velocity skewness, while cooler (blue) colors represent negative vertical velocity skewness. The estimated CBL height is illustrated by an asterisk (*), and aerosol depth is illustrated by an open circle (o). The x-axis represents local time (PDT), and the y-axis depicts the height (m MSL).

An example of a negative SK profile is found in Figure 5. Blue, indicating negative SK, dominates the profile at night, particularly between 400 m MSL and the AD near 700 m MSL from about 0330-0800 PDT. This elevated layer of negative SK represents the "upside-down" profile. It is possible that the source of turbulence is due to an elevated cloud layer at or slightly above this region of negative SK.

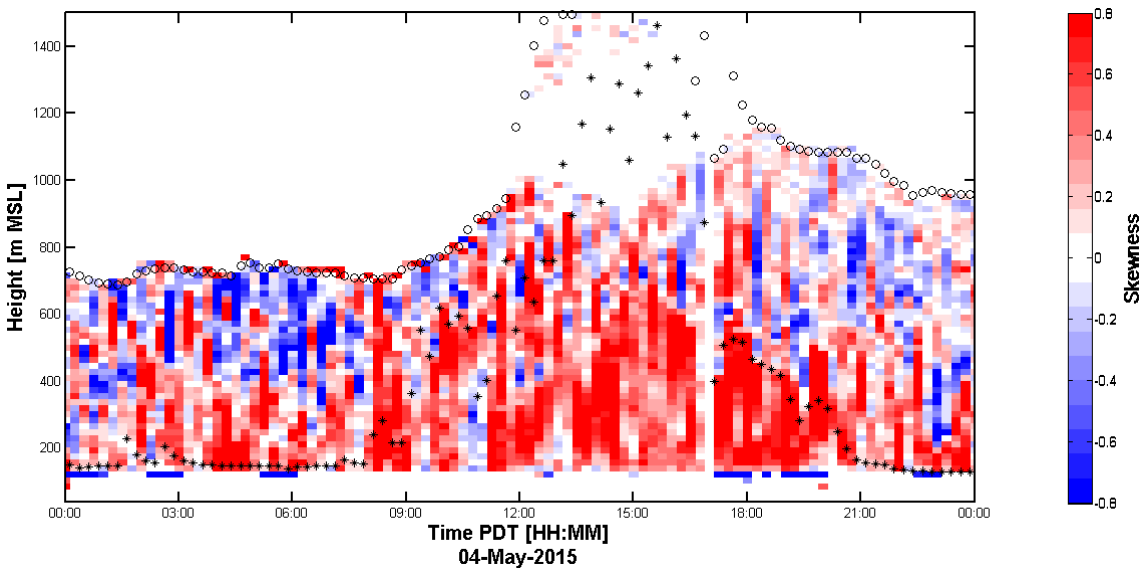

Figure 5: Vertical velocity skewness profile using Doppler LiDAR at SJSU on 04 May 2015. Warmer (red) colors represent positive vertical velocity skewness, while cooler (blue) colors represent negative vertical velocity skewness. The estimated CBL height is illustrated by an asterisk (*), and aerosol depth is illustrated by an open circle (o). The x-axis represents local time (PDT), and the y-axis depicts the height (m MSL).

4. Case Study: Three Common Types of the Boundary Layer

In this chapter we examine the synoptic conditions over San Jose, California, and the influence that a thermal trough brings to the local PBL. The case study consists of an analysis of synoptic conditions from 29 April 2015 to 04 May 2015. Also discussed in this chapter is a case study of three common types of the PBL in San Jose, California using Doppler LiDAR observations at SJSU during the aforementioned synoptic period.

a. Synoptic Summary

Synoptic conditions are examined using isobaric charts, surface weather observations at station SJS01 in San Jose, California, and radiosonde observations from nearby Oakland, California. Synoptic weather conditions impact the structure of the CBL. The PBL is continually in flux and can mold from being a suppressed CBL with shallow

depths due to strong marine influences, to a CBL consisting of a deep ML containing surface-based convective mixing. A synoptic summary begins 29 April 2015.

On 29 April 2015, the 1200 Coordinated Universal Time (UTC) OAK atmospheric sounding illustrated in Figure 6a depicts a mostly saturated atmosphere from the surface to about 950 hPa. A strong inversion layer is located aloft. These temperature inversions are common within a MBL. Predominantly west winds are found through the entire vertical profile from the surface to approximately 300 hPa. The geopotential heights at the 925hPa level in Figure 7a indicate a high pressure in the east Pacific and low pressure in the southwestern United States (centered over southern California). The thermal trough is not yet well established over the Pacific Coast.

On 30 April 2015 at 1200 UTC, a closed low at 925hPa is located near coastal southern California as illustrated in Figure 7b. Also seen in Figure 7b is an inverted trough, or west coast thermal trough (WCTT) (Brewer et al., 2012), lying to the west of California nearly parallel to the coastline. The WCTT is an inverted pressure trough (Brewer et al., 2012). The name thermal trough could be confusing as it is characterized by a thermal ridge of higher temperature in the lower troposphere (Brewer et al., 2012). The OAK atmospheric sounding in Figure 6b suggests the presence of the WCTT off the coast; winds near the surface are therefore easterly over the region bringing warmer and drier continental air to the region, favoring deeper convective mixing. The OAK atmospheric sounding depicts a strong temperature inversion layer at the surface to approximately 925 hPa. This sounding represents a different makeup in the atmosphere, as it lacks the high saturation near the surface compared to the previous day. The WCTT

lying to the west not only impacts the CBL height profile, but it also inhibits the sea breeze circulation pattern over the coastal cities such as nearby San Jose, California. These conditions prohibit a MBL structure from developing over the region. The high temperature in San Jose is depicted in Figure 6a to exceed 30.5 °C. As described in further detail in section 6b, the period of 30 April 2015 at SJSU is an example of a clear CBL with minimal marine influence.

On 01 May 2015, the WCTT moves northeastward and intersects over the California coast and San Jose, as illustrated in Figure 7c. With the northeastward progression and deterioration of the WCTT later in the day, the influence of continental air is reduced. The OAK atmospheric sounding at 1200 UTC 01 May 2015 in Figure 6c shows another strong surface temperature inversion with nearly an absence of easterly winds near the surface. The sounding still lacks a saturated layer near the surface as is evident on 29 April 2015 in Figure 6a before the influence of the WCTT. It is noted in Figure 8 that the local sea breeze circulation pattern is renewed while the maximum temperature at San Jose is reduced to approximately 29 °C.

During the subsequent three days following the exit of the WCTT on 01 May 2015 through 03 May 2015 (Figure 7d, 7e, and 7f), the maximum surface temperature at SJSU decreases (Figure 8a). The maximum temperature was 29 °C on 01 May 2015, 24 °C on 02 May 2015, 23 °C on 03 May 2015, and down to 17.5 °C on 04 May 2015. This is due to a maturing MBL in the bay and a daily sea breeze FROPA interaction. The WCTT is at its apex on 30 April 2015 through 01 May 2015 (Figure 7b and 7c). The WCTT comes

ashore and decays, encouraging the pattern of decreasing temperatures. The details of each subsequent day are expounded upon in the next section of this chapter.

The sea breeze FROPA is a distinct boundary between air masses. Different than the larger-scale sea breeze circulation pattern (or land-sea breeze), the sea breeze FROPA is relatively short, both spatially and temporally. The FROPA is best-defined by a sharp rise in dew point temperature. Other parameters may include a decrease in temperature near the surface and a wind shift. Parameters observed by Doppler LiDAR that suggest a sea breeze FROPA include: a decrease in the CBL height with the intrusion of a MBL, abrupt wind direction shifts (from land to sea breeze) within time scales of 10s of minutes throughout the vertical profile, and wind speed changes in the vertical profile (where an increase is typically seen in San Jose).

It is noted that the OAK atmospheric sounding in Figure 6c lacks a MBL on the morning of 01 May 2015 (likely due to the WCTT located slightly southwest of Oakland). On 02 May 2015 through 04 May 2015 (Figure 6d, 6e, and 6f), a more saturated near-surface environment is evident with higher dew point temperatures beneath a capping inversion layer. The clear CBL structure with minimal marine influence occurs on 30 April 2015, the clear CBL with an afternoon sea breeze is described below for 01 May 2015 through 03 May 2015, while a nocturnal stratocumulus-topped PBL structure is described for 04 May 2015.

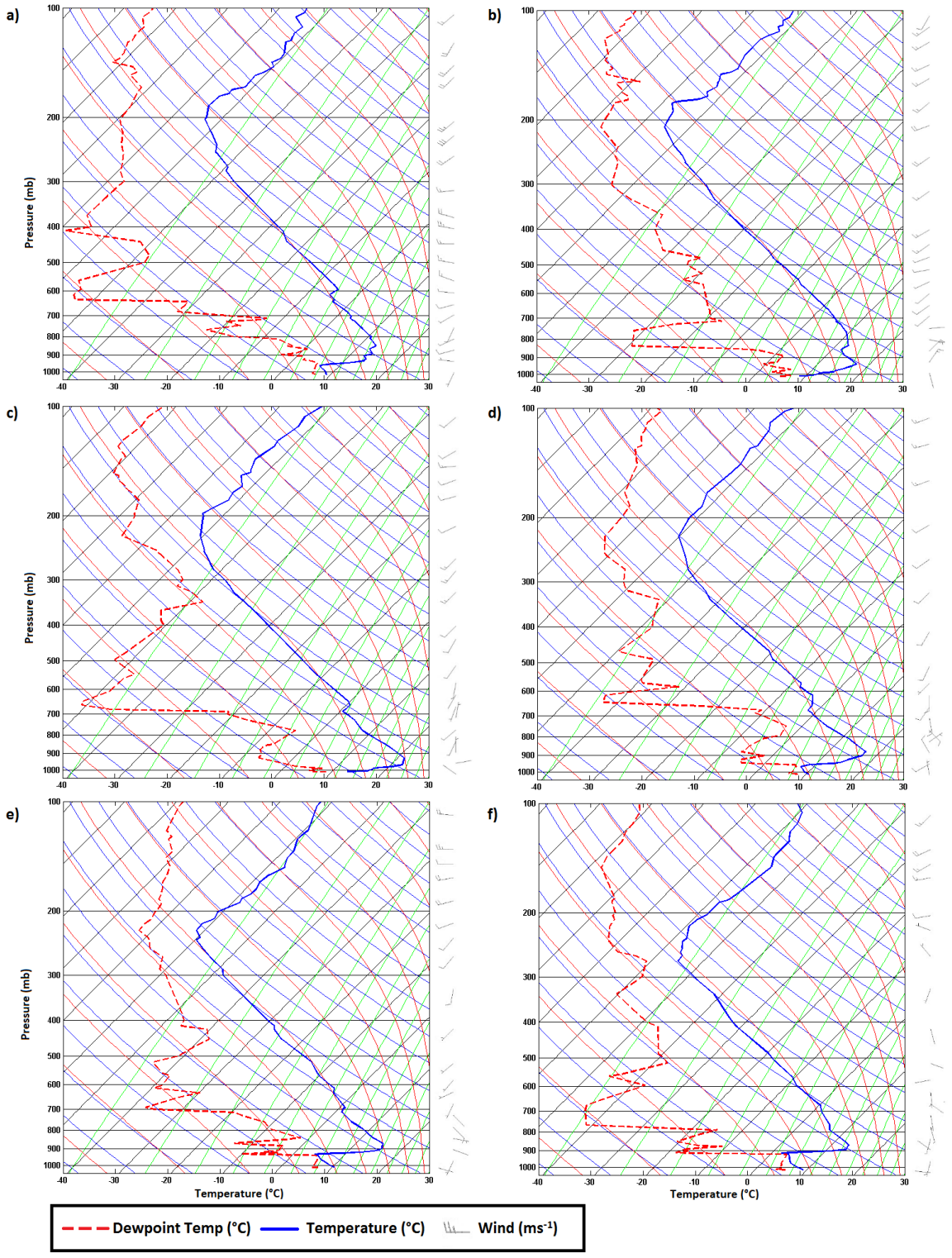

Figure 6: OAK atmospheric soundings 1200 UTC 29 April 2015 - 04 May 2015 (6a-6f).

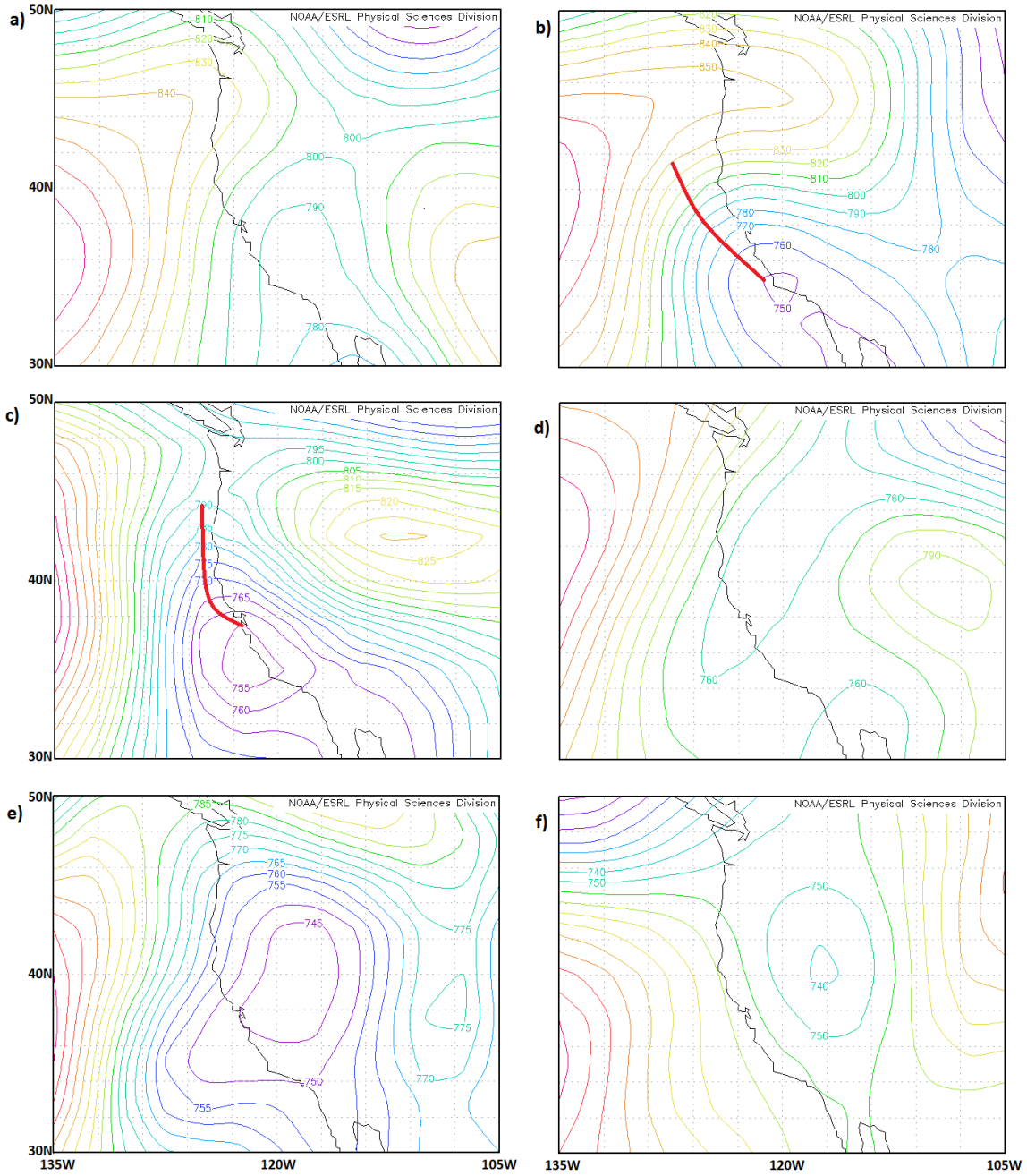

Figure 7: West coast thermal trough (WCTT as solid, bold red line). Geopotential heights (m AGL) at the 925 hPa level (colored contours) over the west coast region of the United States (solid black line) The area lies between 135° W to 105° W and 30° N to 50° N and depicts the date range 29 April 2015 - 04 May 2015 (7a-7f). All times are 1200 UTC.

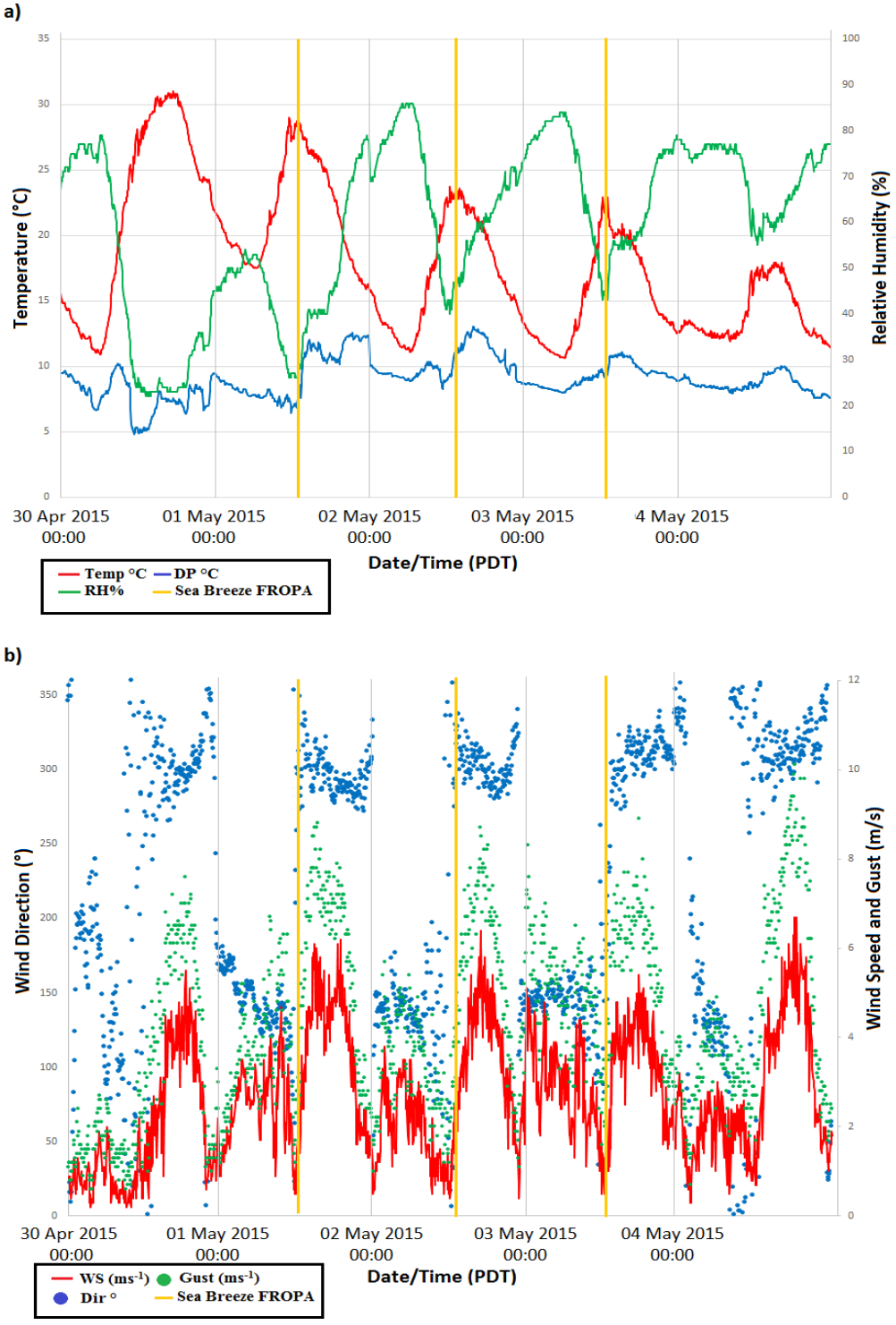

Figure 8: Weather station (SJS01) conditions in San Jose, CA 30 April 2015 – 04 May 2015. Observed temperature (red line Figure 8a), dew point (blue line), wind direction (blue bullets), and wind speed (red line Figure 8b), gusts (green bullets).

b. Daily Doppler LiDAR Observations and Analysis

Doppler LiDAR data are presented in this section detailing the diurnal evolution of the PBL at SJSU, with an emphasis on the estimated CBL height during the day. Three common CBL structures in San Jose, California are: clear convection with minimal marine influence, clear convection with an afternoon sea breeze, and the nocturnal stratocumulus-topped PBL. These are described for the case study on 30 April 2015 through 04 May 2015 in the five examples below. Note that the figures for each day are represented in Pacific Daylight Time (PDT) in order to better visualize the complete diurnal cycle of the CBL.

To introduce the case study, Figure 9 depicts the estimated CBL height (in UTC) from 29 April 2015 through 04 May 2015. This figure summarizes the full period of the case study. The diurnal profile of the estimated CBL height is evident using the σ_w^2 method discussed in the previous chapter. It is noted that the largest values of σ_w^2 occur during the last two days, between approximately 1500 UTC 03 May 2015 and 0000 UTC 04 May 2015 and again at approximately 1500 UTC 04 May 2015 to the end of the period. Values of σ_w^2 approach 1.0 $m^2 s^{-2}$ to heights of approximately 750 m MSL and 500 m MSL, respectively. Another period of higher σ_w^2 occurs between approximately 1500 UTC and 2200 UTC 01 May 2015, with values nearing 1.0 $m^2 s^2$ to heights of approximately 450 m MSL. Note that the elevated, solid black line indicates the estimated CBL height throughout the period in Figure 9. All subsequent figures that include Doppler LiDAR observations utilize the σ_w^2 method described in Chapter 3 to

identify the estimated CBL height. Other parameters were also used to analyze the PBL in the case study between 30 April 2015 and 04 May 2015.

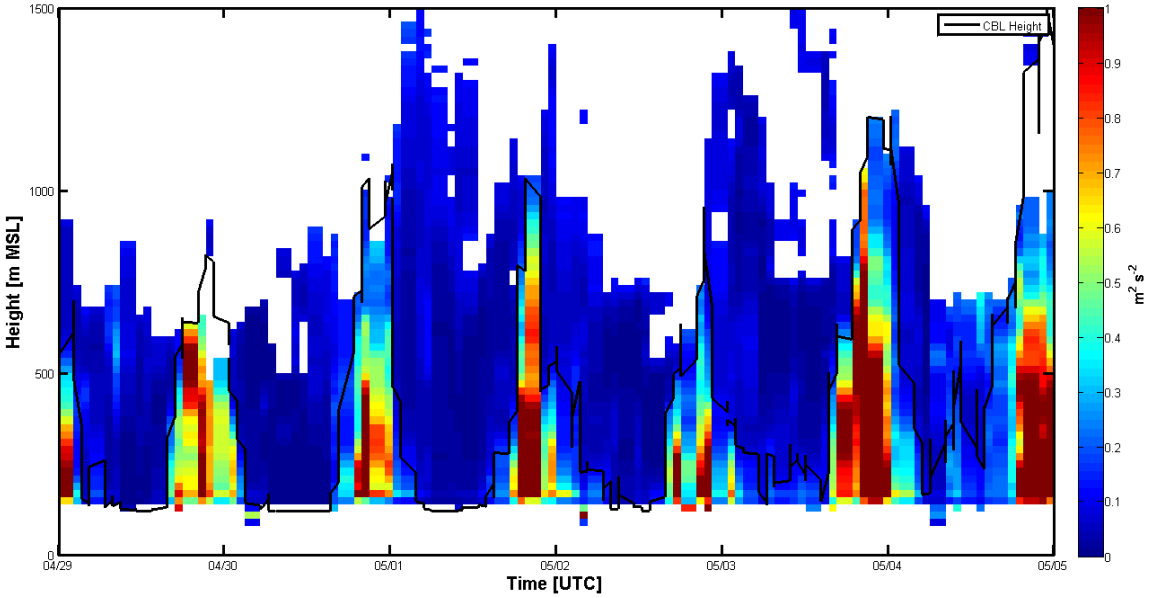

Figure 9: Vertical velocity variance time series. The estimated diurnal CBL height (solid black line) and the σ_w^2 (color shading) for the case study on 29 April 2015 - 04 May 2015. The σ_w^2 has values ranging between 0.0 and 1.0 m^2s^{-2}. The x-axis is time (UTC) as month/day, and the y-axis represents height (m MSL).

1) Clear CBL With Minimal Marine Influence – 30 April 2015

This period on 30 April 2015 exemplifies a clear CBL with minimal marine influence during the daytime in San Jose. Sunrise is approximately 0614 PDT and sunset is about 1956 PDT. The first detectable growth of the CBL begins close to 0900 PDT, with the CBL growing slowly at first, then rapidly after 1030 PDT. The CBL reaches heights over 800 m MSL by approximately 1500 PDT and collapses most rapidly at 1630 PDT. The CBL height collapses to near-surface levels after 1800 PDT.

The CBL height is strongly influenced by surface heating, resulting in turbulent conditions throughout the period between sunrise and sunset. In Figure 10, the attenuated

backscatter returns are highest from the surface to approximately 400 m MSL and occur between about 0000 PDT and 1000 PDT. In this region, the aerosol returns approach -4.5 m^{-1} sr^{-1}. It is not conclusive that clouds are present because the Doppler LiDAR does not attenuate entirely. However, this signal could be due to swollen aerosol. According to Engelmann et al. (2008), cloud droplets can form on the swollen aerosol particles impacting the Doppler LiDAR return. On the contrary, the dry tropospheric air from the FA is a factor for growth and shrinking particles (Engelmann et al. 2008). This affects the apparent particle mass concentration.

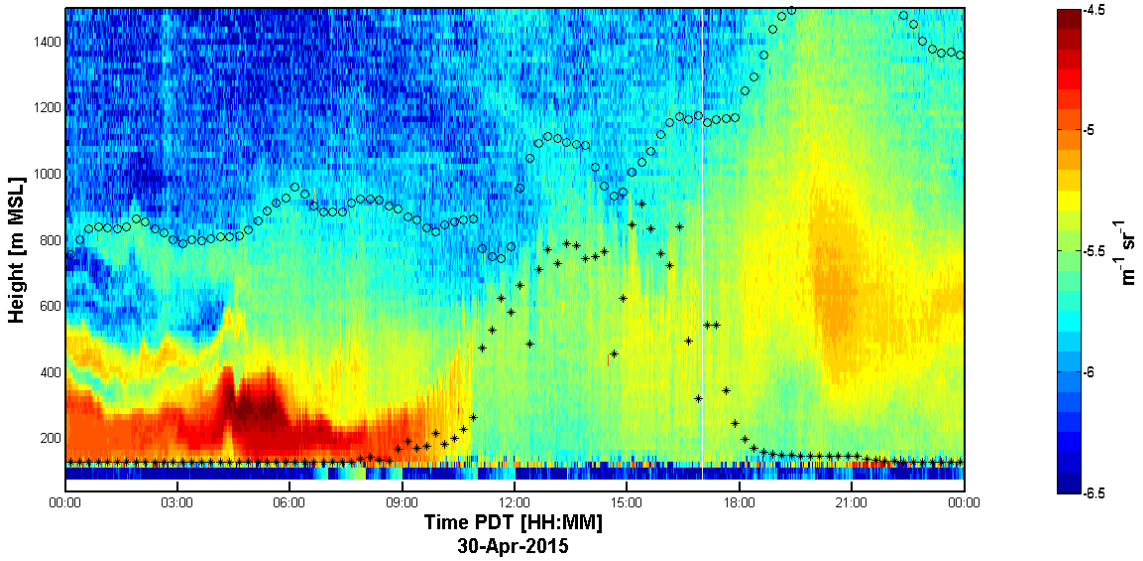

Figure 10: Attenuated backscatter profile using Doppler LiDAR at SJSU on 30 April 2015. Warmer (red and orange) colors represent a more positive backscatter (m^{-1} sr^{-1}), while cooler (blue) colors represent more negative backscatter. The estimated CBL height is illustrated by an asterisk (*), and aerosol depth is illustrated by open circles (o). The x-axis represents local time (PDT), with y-axis depicting the height (m MSL).

It is noted that the parameter, AD, in Figure 10 is the uppermost edge of aerosol backscatter identified in the CBL profile. In essence, the AD is identified as the upper bound that the Doppler LiDAR returns can collect. This threshold helps identify where

the aerosol is not present above that given level. Below the AD mark is typically representative of valid data; whereas above the AD, the returns are often sparse and contain a majority of missing data that might not be validated toward any analysis. At times, the estimated CBL height and AD coincide, indicating a possible obstruction such as optically thick clouds. The AD parameter is identified in all of the Doppler LiDAR figures.

It is noted that a decoupling of a shallow aerosol backscatter layer is returned by the Doppler LiDAR from the beginning of the period until approximately 0430 PDT between 400-600 m MSL. Backscatter returns in this thin layer are near -5.25 m^{-1} sr^{-1}. Backscatter returns within the CBL in the daytime are lower, near -5.75 to -5.4 m^{-1} sr^{-1}, and up to approximately -5.1 m^{-1} sr^{-1} in the elevating RL.

The minimum and maximum returns of vertical velocity are presented in Figure 11 within the CBL through the daytime hours. Updraft and downdraft velocities of -2 m s^{-1} and 2 m s^{-1} are observed. It is noted that the vertical velocity profile in Figure 11 suggests the formation of a RL following the peak estimated CBL height between 1600 PDT and 1900 PDT at 800 m MSL up to approximately 1400 m MSL.

The maximum values of σ_w^2 in Figure 12 are evident between the surface and approximately 600 m MSL within the CBL, occurring between about 1100 PDT and 1700 PDT. Deep, convective mixing of the CBL to heights of 700-800 m MSL occurs in the mid-afternoon, as illustrated by the σ_w^2. It is also noted that the upward propagating region previously discussed with vertical velocity, is also evident in the σ_w^2 between

1800 PDT and 1900 PDT at approximately 1200 m MSL. The σ_w^2 approaches values of 0.75 m^2 s^{-2} near this elevated region of the RL.

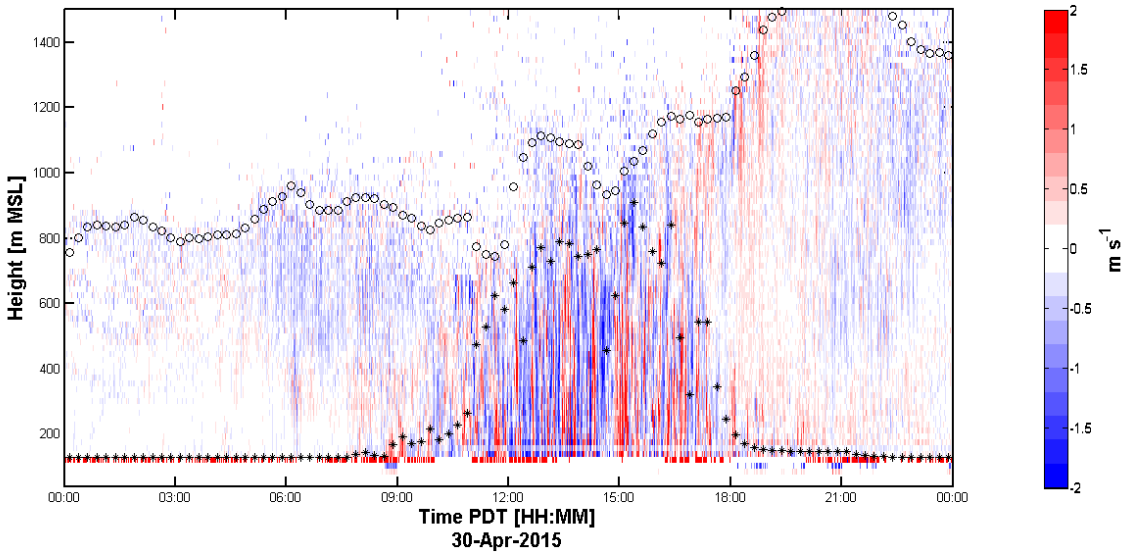

Figure 11: Vertical velocity profile using Doppler LiDAR at SJSU on 30 April 2015. Warmer (red) colors represent positive (upward) vertical velocity (m s^{-1}), while cooler (blue) colors represent negative (downward) vertical velocity. The estimated CBL height is illustrated by an asterisk (*), and aerosol depth is depicted by an open circle (o). The x-axis represents local time (PDT), with y-axis depicting the height (m MSL).

Figure 13 illustrates the SK as dominantly positive within the daytime CBL, indicating a clear CBL. Peak afternoon positive SK occurs above 400 m MSL, but remains predominantly below 700 m MSL. As previously mentioned with respect to Figure 11, within the RL is an elevated maxima of vertical velocity; simultaneously in Figure 13 is a maxima of positive SK at approximately 1800 PDT and exceeding 1000 m MSL. Some negative SK is noted in the early morning hours, possibly indicating a low cloud base before sunrise. Most of the regions of negative SK in the early morning hours are located at or below 400 m MSL. However, some small sections of negative SK are located near 600 m MSL.

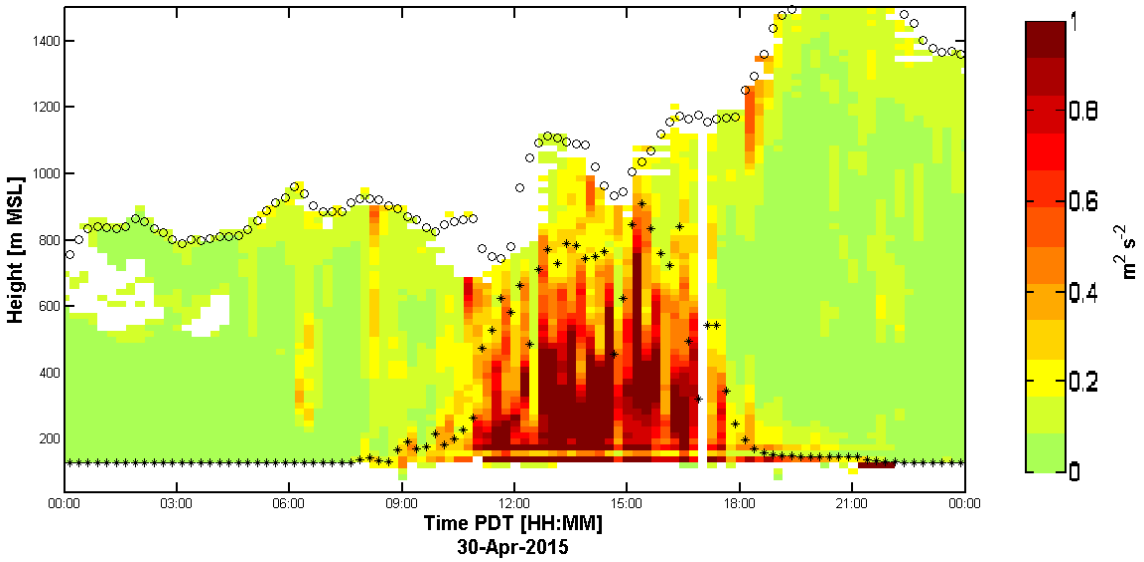

Figure 12: Vertical velocity variance derived from Doppler LiDAR at SJSU on 30 April 2015. Warmer (red and orange) colors represent a more positive vertical velocity variance (m^2 s^{-2}), while cooler (green) colors are lower values. The estimated CBL height is illustrated by an asterisk (*), and aerosol depth is illustrated by an open circle (o). The x-axis represents local time (PDT), and the y-axis depicts the height (m MSL).

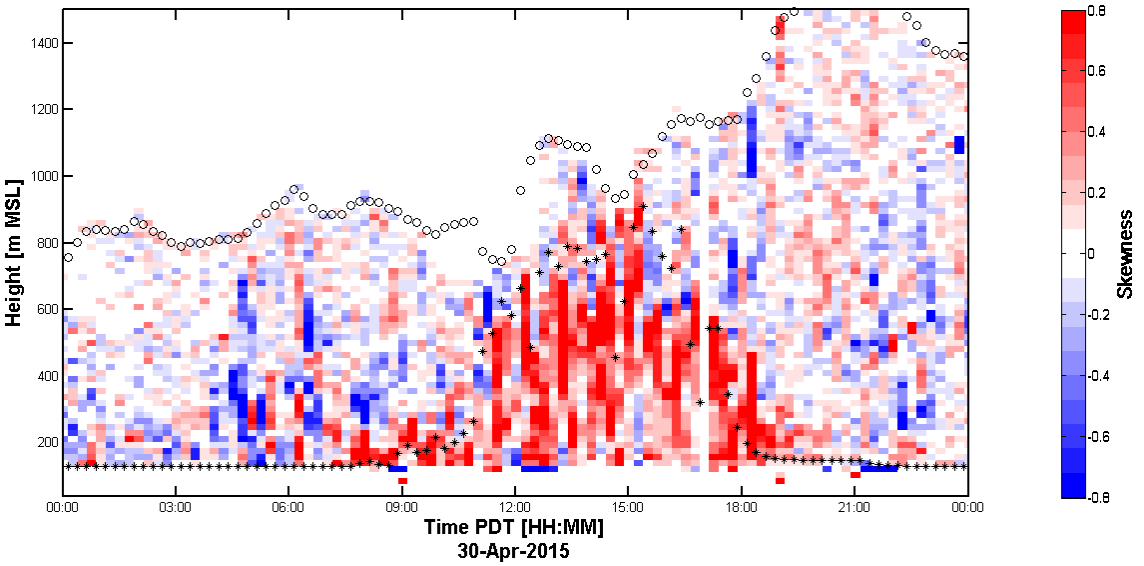

Figure 13: Vertical velocity skewness profile using Doppler LiDAR at SJSU on 30 April 2015. Warmer (red) colors represent positive vertical velocity skewness, while cooler (blue) colors represent negative vertical velocity skewness. The estimated CBL height is illustrated by an asterisk (*), and aerosol depth is illustrated by an open circle (o). The x-axis represents local time (PDT), and the y-axis depicts the height (m MSL).

Winds are light and variable near the surface between 0000 PDT and 1200 PDT with speeds typically below 3 m s^{-1} as depicted in Figure 14. An elevated wind speed maximum is located near 600 m MSL from 0500 PDT to 0930 PDT, bringing continental air from the California Central Valley (CCV) in a northeasterly flow as illustrated in Figure 15. As the CBL matures through the afternoon, the winds become less variable. Thermally driven, larger-scale circulations influence air flow toward Gilroy (see Figure 2 for the location) to the southeast, whereas winds near the surface are predominantly northwesterly by approximately 1400 PDT.

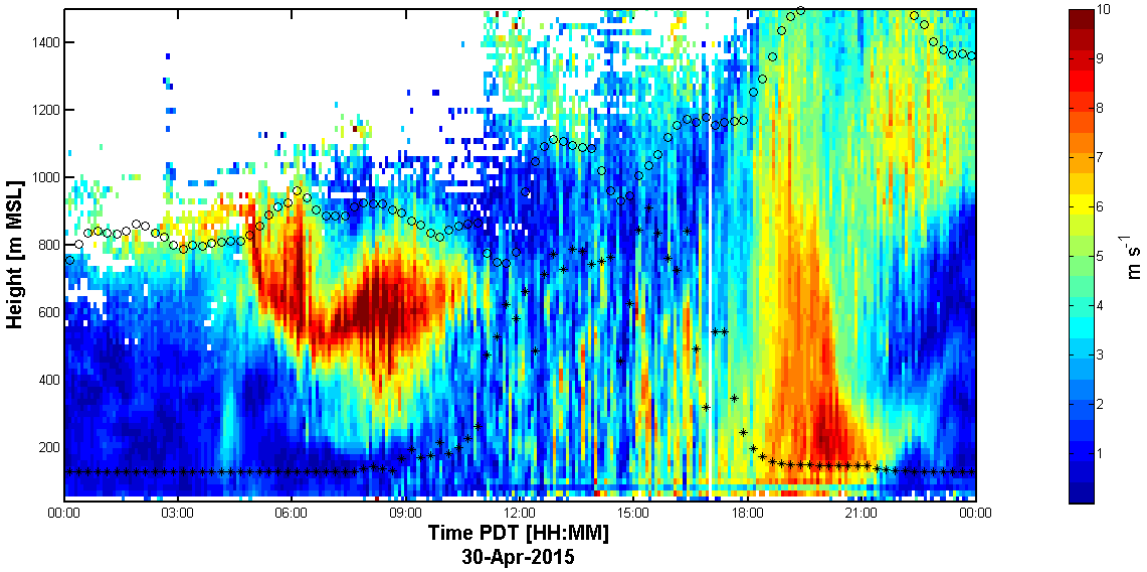

Figure 14: Wind speed profile using Doppler LiDAR at SJSU on 30 April 2015. The estimated CBL height is illustrated by an asterisk (*), and the estimated aerosol depth is illustrated by an open circle (o). The x-axis represents local time (PDT), with y-axis depicting the height (m MSL).

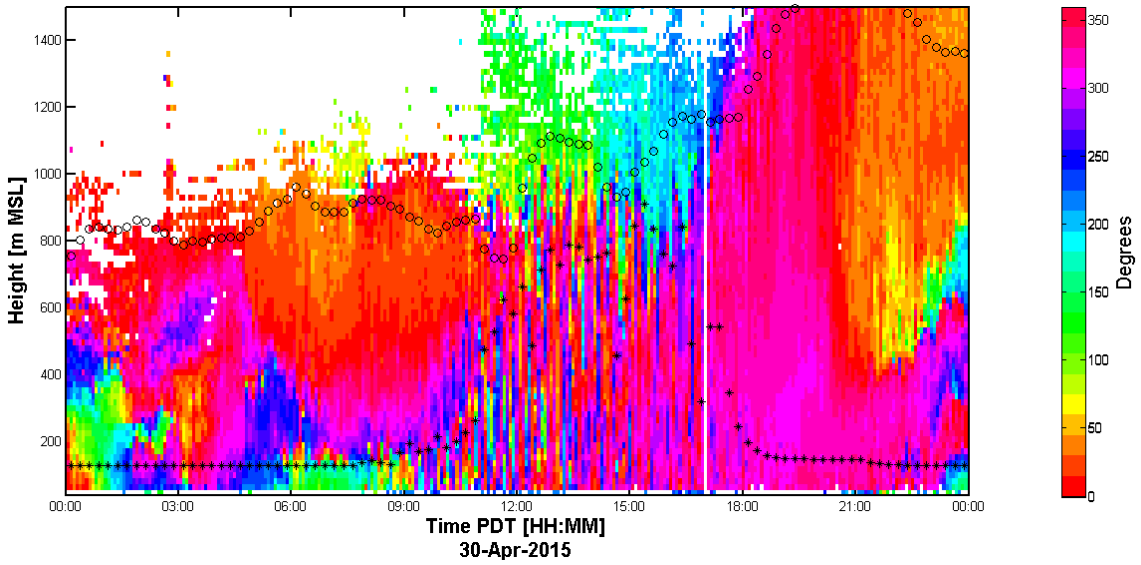

Figure 15: Wind direction profile using Doppler LiDAR at SJSU on 30 April 2015. The estimated CBL height is illustrated by an asterisk (*), and the estimated aerosol depth is illustrated by an open circle (o). The x-axis represents local time (PDT), with y-axis depicting the height (m MSL).

The RL is present immediately following the collapse of the CBL. Coinciding with northwesterly winds of approximately 5-8 m s^{-1}, residual turbulence is reduced, yet it evidently propagates vertically to approximately 1500 m MSL between approximately 1630 PDT and 2200 PDT. The RL exceeds heights of the preceding CBL height maximum of approximately 700-800 m MSL. This vertical propagation is a result of the rapid CBL height growth, deep convective turbulent mixing, and entrainment of air from the ML into the FA. In the RL, the vertical velocity in Figure 11 is lower than within the CBL, with values near +/- 0.5 ms^{-1}, the σ_w^2 approaches 0 to 0.1 m^2 s^{-2}, and the SK becomes more neutral. The RL persists into the next day as the AD (open circles) is indicated in Figure 10-15.

The SJS01 surface atmospheric observations in Figure 8 indicate temperatures beginning near 11 degrees Celsius (°C) at sunrise and quickly reaching over 30 °C by

approximately 1500 PDT - near the same time as the CBL's maximum height on 30 April 2015. This swing in temperature is mirrored with a reduction in relative humidity (RH) from 80% to below 25% and a decrease in dew point temperature from 10 °C to 5 °C as surface winds near 2 ms^{-1} out of the east advect a drier air mass to San Jose. The SJS01 data, in connection with the Doppler LiDAR observations, strongly suggest 30 April 2015 as an example of a clear CBL with minimal marine influence. This type of CBL structure is due to the approach and passage of the WCTT. This occurrence, as shown in Figure 7b, is depicted as the inverted pressure trough remains offshore on 30 April 2015. The observed near-surface easterly and northeasterly winds before sunrise are evidence of the offshore flow. This continental influence minimizes any effects of a MBL, therefore no afternoon sea breeze is captured by the data.

This period, 30 April 2015, represents a clear CBL with minimal marine influence. An uncertain backscatter layer near the surface in the pre-dawn hours may cause speculation of low-level clouds or light mist and fog. However, high surface temperatures exceeded 30 °C due to the offshore passage of a developing WCTT in Figure 7a.Then as a mature inverted trough in Figure 7b parallels the coast, it is suggested that the continental influence produces a PBL with minimal cloud cover throughout the daytime. Further evidence of surface-based heating of the CBL in Figure 13 is illustrated by a predominantly positively skewed profile, indicated by narrow updrafts and broad downdrafts.

2) Clear CBL With Afternoon Sea Breeze Frontal Passage – 01 May 2015

This period on 01 May 2015 illustrates the development of a clear CBL with an afternoon sea breeze FROPA and MBL influence. The approximate times for sunrise and sunset are 0613 PDT and 1957 PDT, respectively. The CBL growth initiates at approximately 0830 PDT. The CBL grows simultaneously with the southeasterly drainage flow (Figure 16 and 17). A rapid increase in the CBL height occurs in the morning hours, peaking near 950 m MSL shortly after 1200 PDT. This peak is short-lived, as the CBL height collapses to approximately 230 m MSL at 1500 PDT. The CBL height grows briefly to 400 m MSL at approximately 1630 PDT before collapsing again in the early evening hours. By 1830 PDT, the CBL height is relaxed from daytime convective mixing and collapses near the surface.

The most vigorous mixing occurs near the daily maximum CBL height. Likewise, the σ_w^2 profile in Figure 18 depicts the highest values of 0.8-1.0 $m^2 s^{-2}$ near the time of the peak CBL height, representative of this well-mixed CBL. The greatest values of vertical velocity are evident during this time, as portrayed in Figure 19, near the peak CBL height. The strongest updrafts tend to be narrower and more intense than the broader, weaker downdrafts that follow (Hogan et al. 2009).

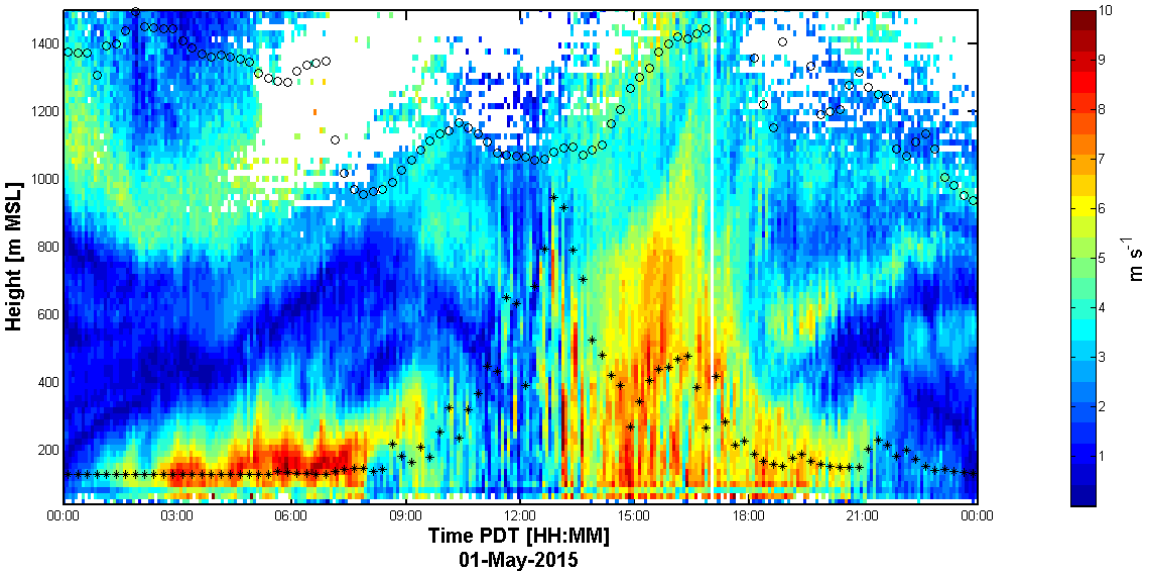

Figure 16: Wind speed profile using Doppler LiDAR at SJSU on 01 May 2015. The estimated CBL height is illustrated by an asterisk (*), and the estimated aerosol depth is illustrated by an open circle (o). The x-axis represents local time (PDT), with y-axis depicting the height (m MSL).

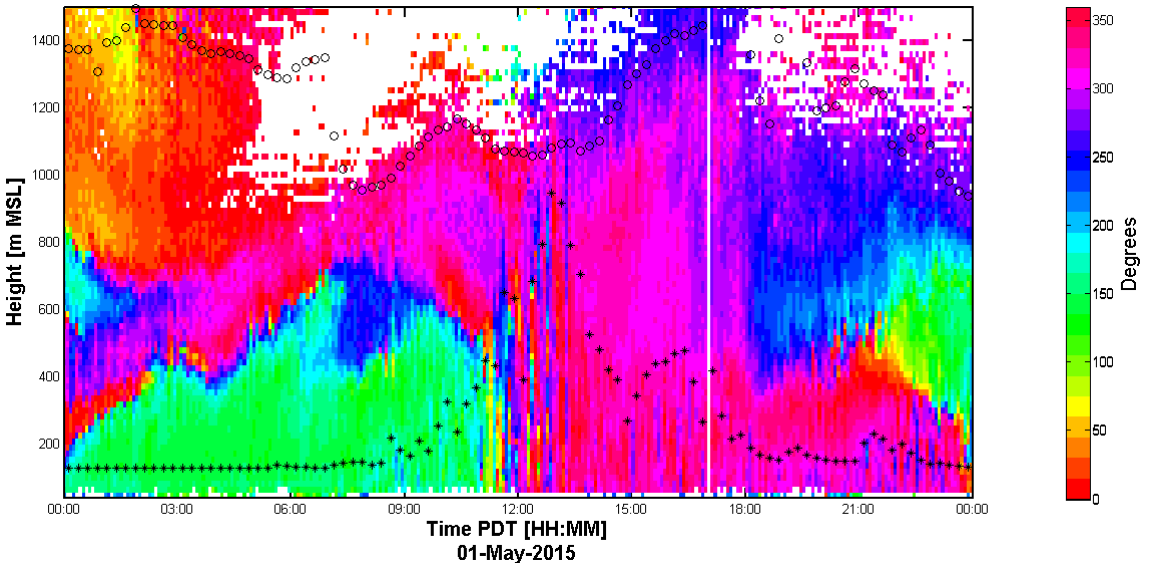

Figure 17: Wind direction profile using Doppler LiDAR at SJSU on 01 May 2015. The estimated CBL height is illustrated by an asterisk (*), and the estimated aerosol depth is illustrated by an open circle (o). The x-axis represents local time (PDT), with y-axis depicting the height (m MSL).

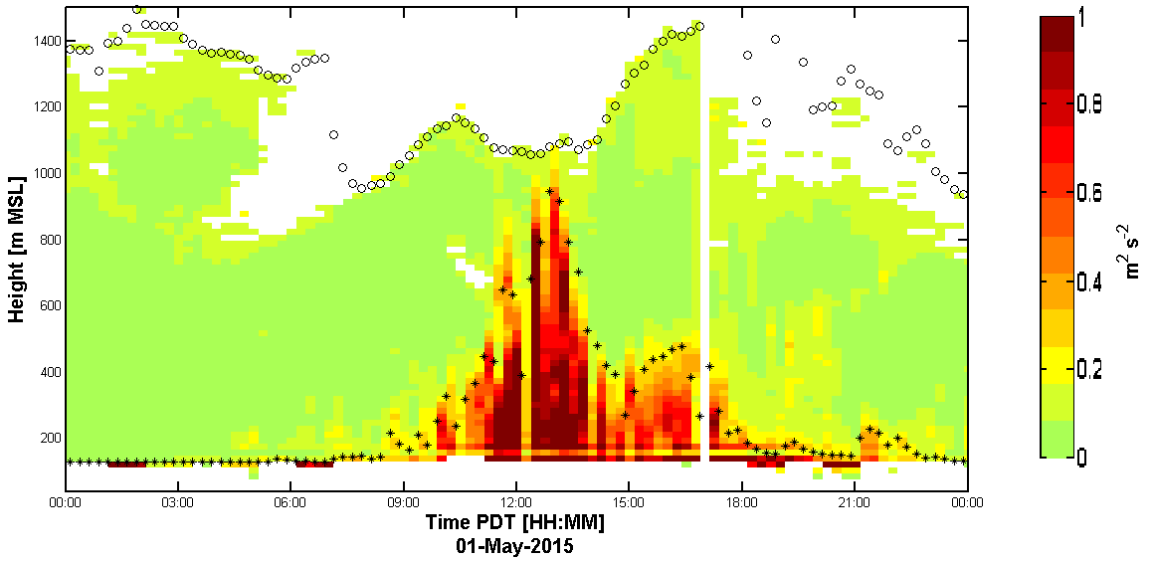

Figure 18: Vertical velocity variance derived from Doppler LiDAR at SJSU on 01 May 2015. Warmer (red and orange) colors represent a more positive vertical velocity variance (m^2 s^{-2}), while cooler (green) colors are lower values. The estimated CBL height is illustrated by an asterisk (*), and aerosol depth is illustrated by an open circle (o). The x-axis represents local time (PDT), and the y-axis depicts the height (m MSL).

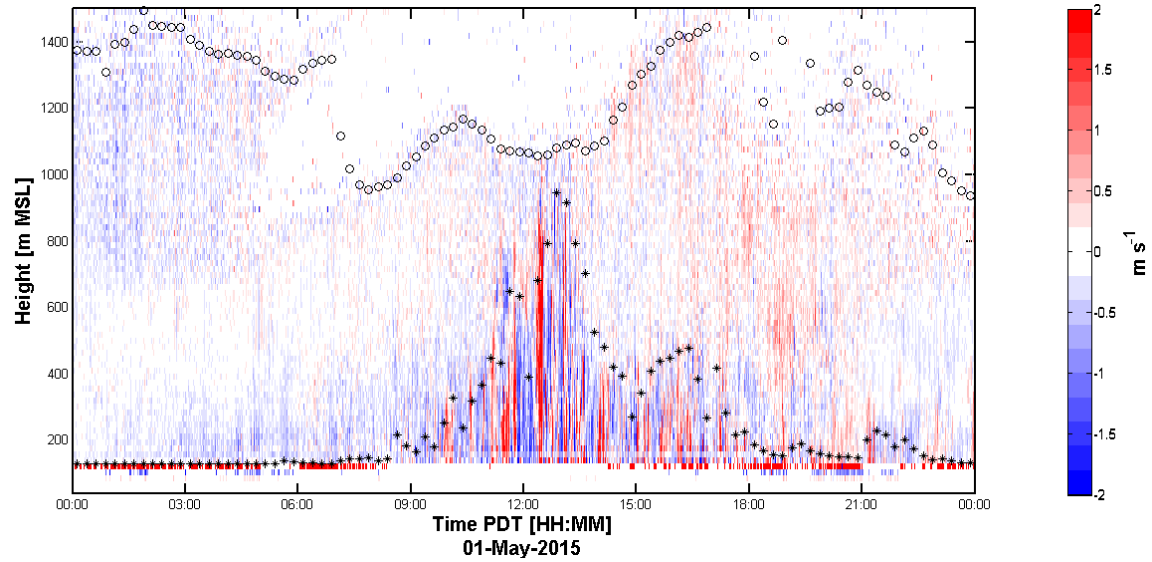

Figure 19: Vertical velocity profile using Doppler LiDAR at SJSU on 01 May 2015. Warmer (red) colors represent positive (upward) vertical velocity (m s^{-1}), while cooler (blue) colors represent negative (downward) vertical velocity. The estimated CBL height is illustrated by an asterisk (*), and aerosol depth is depicted by an open circle (o). The x-axis represents local time (PDT), with y-axis depicting the height (m MSL).

The diurnal sea breeze circulation pattern is a common occurrence for the San Jose region. During the afternoon hours, assuming the absence of significant cloud cover or synoptic disturbances, the initialization of the sea breeze circulation pattern occurs due to a greater *H* over land than that over the water. The stronger convective mixing over the land results in a sea breeze (Holton 1972) in San Jose. This, in association with along-valley and upslope flows to the south of San Jose, is the cause of the climatological northwesterly winds in the afternoon. In the evening through the morning hours, the sea breeze circulation pattern is reversed. Surface cooling over land is greater than that over the water. The along-valley flows, associated with the downslope flows surrounding San Jose to the south and southeast, aid in the reversal of the circulation pattern. With the absence of solar radiation, terrain flows perpetuate the land breeze as the southeasterly winds ensue.

In Figure 20, a higher backscatter return is evident at about 600 m MSL at the beginning of the period. This RL of aerosol lingers from the previous day's turbulent activity. The rapid increase in the CBL height is followed by an increase of the AD. Between approximately 1200 PDT and 1630 PDT, the AD increases over 300 m to about 1450 m MSL.

The conditions during the peak CBL height are indicative of a surface-heating-driven CBL resulting in a positively skewed region (see Figure 21). The SK profile displays a CBL profile with a positive SK within the CBL, despite the relatively brief elevation of the CBL height around 1200 PDT.

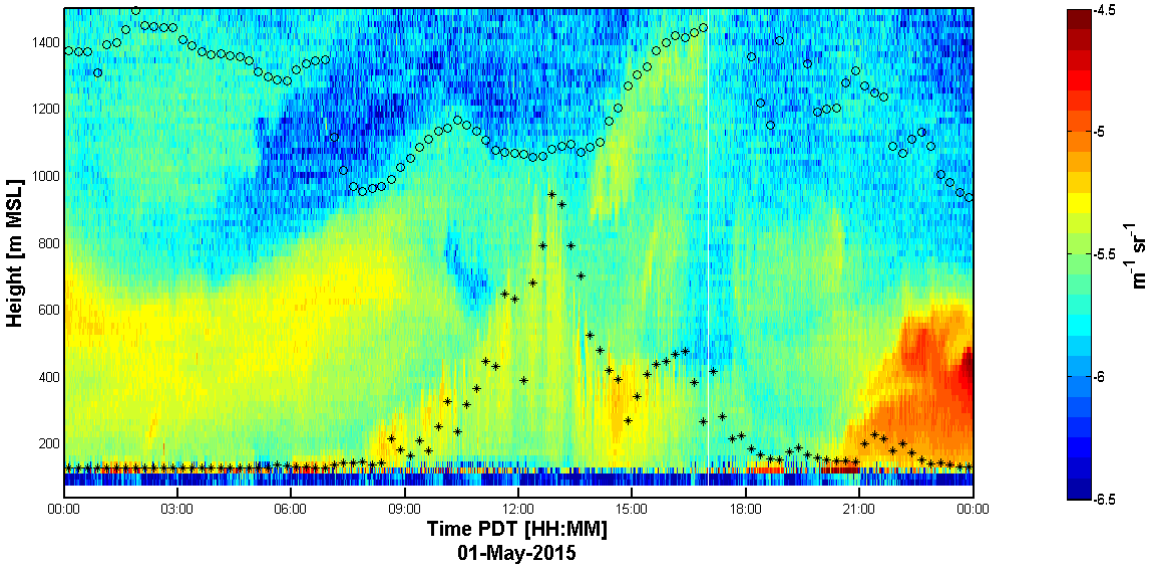

Figure 20: Attenuated backscatter profile using Doppler LiDAR at SJSU on 01 May 2015. Warmer (red and orange) colors represent a more positive backscatter (m^{-1} sr^{-1}), while cooler (blue) colors represent more negative backscatter. The estimated CBL height is illustrated by an asterisk (*), and aerosol depth is illustrated by open circles (o). The x-axis represents local time (PDT), with y-axis depicting the height (m MSL).

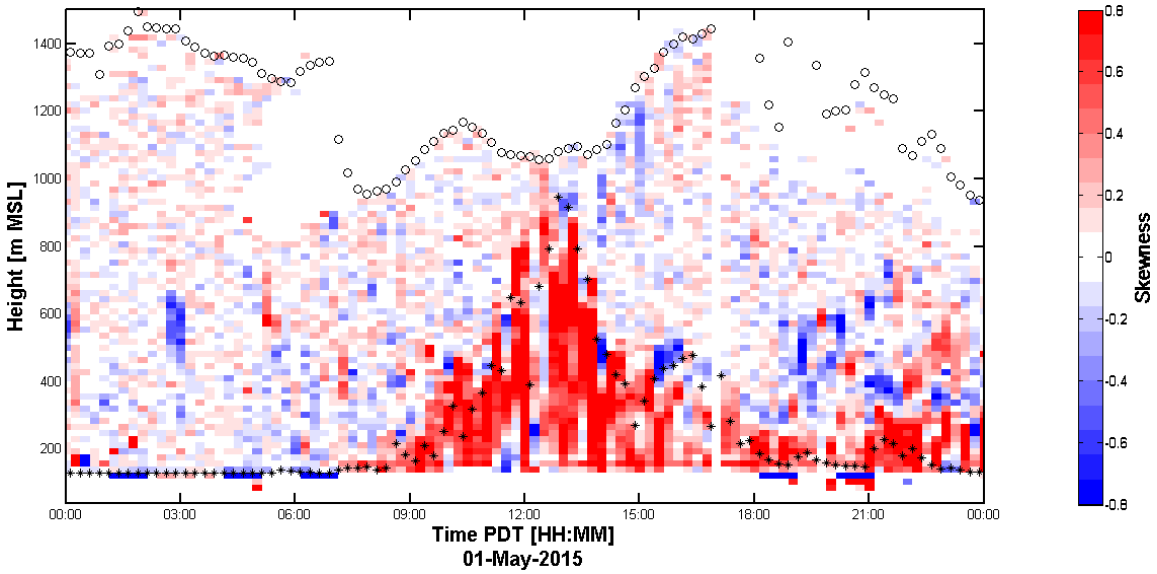

Figure 21: Vertical velocity skewness profile using Doppler LiDAR at SJSU on 01 May 2015. Warmer (red) colors represent positive vertical velocity skewness, while cooler (blue) colors represent negative vertical velocity skewness. The estimated CBL height is illustrated by an asterisk (*), and aerosol depth is illustrated by an open circle (o). The x-axis represents local time (PDT), and the y-axis depicts the height (m MSL).

The abrupt collapse of the CBL height in the early afternoon is explained in the timing of the sea breeze FROPA. Surface weather observations from SJS01 depict a low temperature near 17.6 °C at 0615 PDT (near local sunrise) and a high temperature of 29 °C at 1135 PDT. The increase in surface temperature occurs in concert with the increase in CBL height, suggesting a typical clear CBL evolution up to this time. The temperature time series in Figure 8 clearly illustrates the arrival of a new air mass, a MBL, as temperatures fall 2.4 °C from 1310 PDT to 1435 PDT. Simultaneously, the dew point temperature increases 3.3 °C. The increase in dew point temperature is one indicator of the marine origins of this air. Similarly, the wind time series in Figure 8 indicates the timing of arrival of the sea breeze FROPA near the surface.

During the first 12 h of the period in Figure 16 and 17, southeasterly winds up to approximately 9 m s^{-1} represent a drainage flow. The winds shift to northwesterly and increase in speed, defining the sea breeze FROPA. The sea breeze FROPA corresponds with the observed CBL height decrease of 700 m in 2.5 h, as it represents the intrusion of a MBL.

The arrival of the sea breeze FROPA precludes further CBL height development due to differential cold air advection. The CBL becomes more stabilized as the MBL intrudes near the bottom of the original CBL. This restricts the ability for deep thermals to develop. The absence of the stronger thermals results in the lack of a more established CBL that is expected over land-based surface heating. In Figure 22, the expected structure of a clear CBL with a sea breeze FROPA is illustrated. Notice the suppression that is portrayed in the CBL height following the sea breeze FROPA from the north. It is

speculated, due to repeated Doppler LiDAR observations, that this occurs due to differential cold air advection (analogous to the MBL identified in Figure 22). As the CBL becomes more stabilized, with the arrival of the MBL from the San Francisco Bay, land-based heating within the profile become less influential on the CBL height growth.

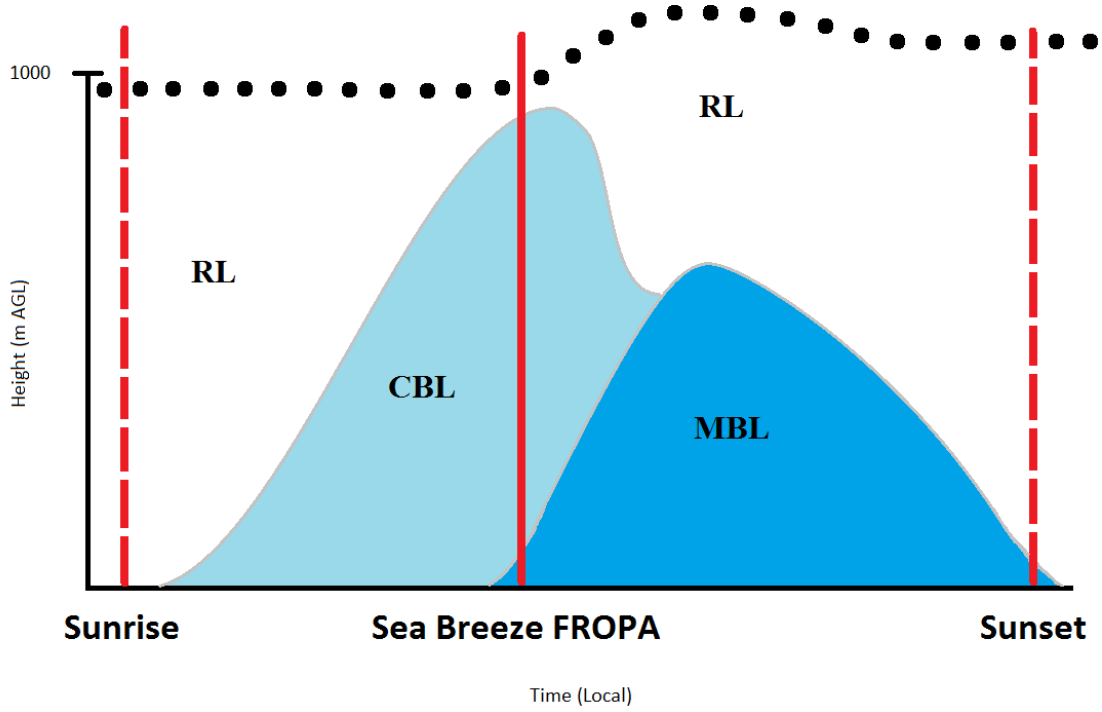

Figure 22: Clear CBL diurnal pattern with a sea breeze frontal passage (FROPA) in San Jose, California. Components of the PBL: residual layer (RL), convective boundary layer (CBL), and marine-influenced boundary layer (MBL). Sunrise and sunset are identified (red hashed lines) along with the approximate arrival of the sea breeze FROPA (solid red line) and estimated AD (black bullets).

It is also detected in many Doppler LiDAR observations, and noted in Figure 22, that the AD (black bullets) may exhibit an elevated motion following peak CBL height growth. Preceding figures in this section portray this pattern (e.g., see open circles in Figure 21). While the identified AD from Doppler LiDAR observations suggests a pattern of lift following peak CBL height growth, it is noted that this layer is defined by

the sharp decrease in aerosol backscatter. Further case studies may be necessary to draw any conclusions on the upward motion of the AD. However, it is speculated that this is due to a mechanical lifting process. As the wedge of colder air (i.e. the MBL) intrudes, it displaces the full structure of the PBL upward. It may also be the decaying process due to the residual turbulence from the CBL. The CBL decays prematurely because it becomes decoupled by the MBL.

The 01 May 2015 wind speed profile in Figure 16 and wind direction profile in Figure 17 illustrate the regional sea breeze circulation. During the early morning hours before sunrise, near-surface winds are dominantly southeasterly below 400 m MSL until approximately 1100 PDT. From 0300 PDT to 0700 PDT a low-level jet (below 200 m MSL) of nearly 8-9 m s^{-1} indicates a strong land breeze or drainage flow toward the San Francisco Bay to the north. Within the CBL around noon, winds shift from a more westerly to a northerly direction. Following the sea breeze FROPA, the winds are consistently from the northwest. These winds are indicative of the onshore flow coinciding with an up-valley flow toward adjacent Morgan Hill and Gilroy to the southeast and following the larger sea breeze circulation pattern. Similar to the preceding day, Figure 18 indicates a region of reduced turbulent motions following the collapse of the CBL height at approximately 1230 PDT. This region represents the RL that is identified in Figure 1 and 22. The northwesterly flow between the surface to about 1000 m MSL at approximately 5-8 m s^{-1} coincide with a decrease in vertical velocity, σ_w^2 and SK, defining the presence of the RL that persists through the end of the day and into the morning of the next.

To conclude the period for the PBL exhibited here on 01 May 2015, the case study illustrates a clear CBL with an afternoon sea breeze FROPA. The land-sea association is apparent during this period. The sea breeze circulation pattern begins in the pre-dawn hours with a low-level wind speed maximum (as seen in Figure 16) with a southeasterly wind direction (as seen in Figure 17), indicating a drainage flow along-valley from the Gilroy area to the San Francisco Bay. As surface-based heating ensues in the daytime, the CBL height grows rapidly preceding the arrival of a sea breeze FROPA in the early afternoon. This results in decreased temperature and increased humidity at SJS01. Immediately following the sea breeze FROPA, the CBL height is suppressed to nearly one-fourth the peak height before increasing briefly later in the afternoon. The MBL inundates the CBL, essentially decoupling the source of turbulence. The source of turbulence may be land-based, or in the case of a MBL, turbulence is often advected into the profile. Winds are predominantly northwesterly through the latter part of the day as the sea breeze dominates. A diurnal circulation pattern ensues through 03 May 2015. It is estimated that the WCTT passes ashore in San Jose during the afternoon hours, as Figure 7c illustrates an arrival at approximately 1200 UTC to the San Francisco Bay in proximity to the Pacific Ocean coastline. This is indicated by increased dew point temperatures in the following evening on 02 May 2015 as a MBL encapsulates the diurnal profile through the following days. It is also noted that daytime high temperatures begin a steady decrease through 04 May 2015. With the absence of the WCTT off the Pacific coast, the MBL is more influential to the diurnal profile at San Jose.

3) Clear CBL With Afternoon Sea Breeze Frontal Passage – 02 May 2015

This period on 02 May 2015 also exemplifies a clear CBL with an afternoon sea breeze FROPA and a MBL influence in San Jose. Sunrise is 0612 PDT and sunset is 1958 PDT. As illustrated by the vertical velocity profile in Figure 23 and the σ_w^2 values in Figure 24, the initial growth of the CBL occurs at approximately 0730 PDT. A rise of the CBL height to about 500 m MSL occurs at 1100 PDT, and then it subsides about 100 m by 1200 PDT. CBL height increases again, reaching its daily maximum of 800 m MSL around 1330 PDT. A rapid collapse of the CBL height ensues to approximately 250 m MSL at 1600 PDT. After a brief increase in height, the CBL gradually subsides to near-surface levels after 2100 PDT.

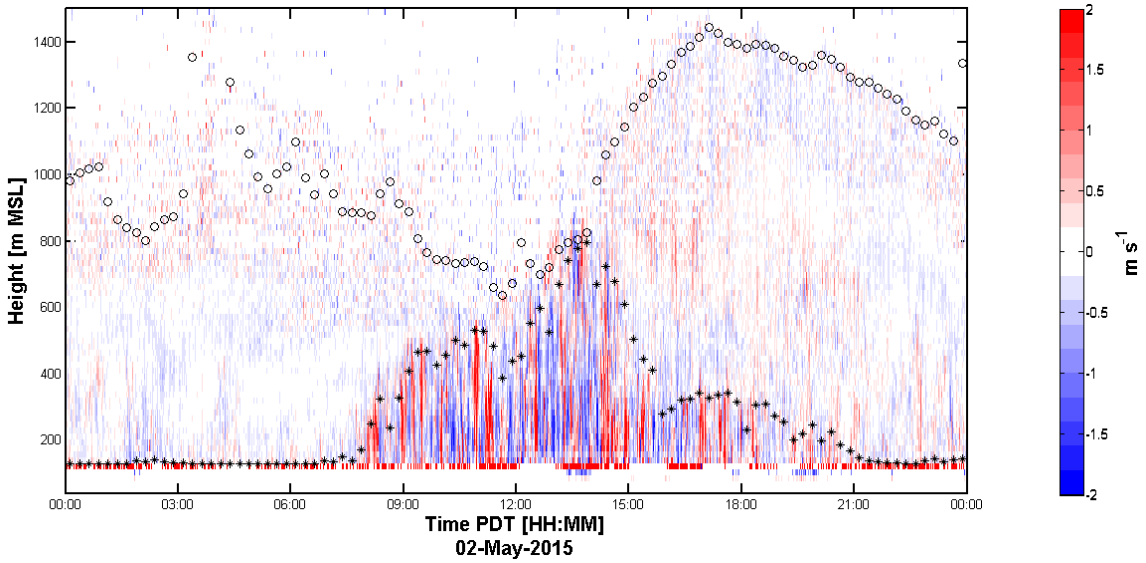

Figure 23: Vertical velocity profile using Doppler LiDAR at SJSU on 02 May 2015. Warmer (red) colors represent positive (upward) vertical velocity (m s^{-1}), while cooler (blue) colors represent negative (downward) vertical velocity. The estimated CBL height is illustrated by an asterisk (*), and aerosol depth is depicted by an open circle (o). The x-axis represents local time (PDT), with y-axis depicting the height (m MSL).

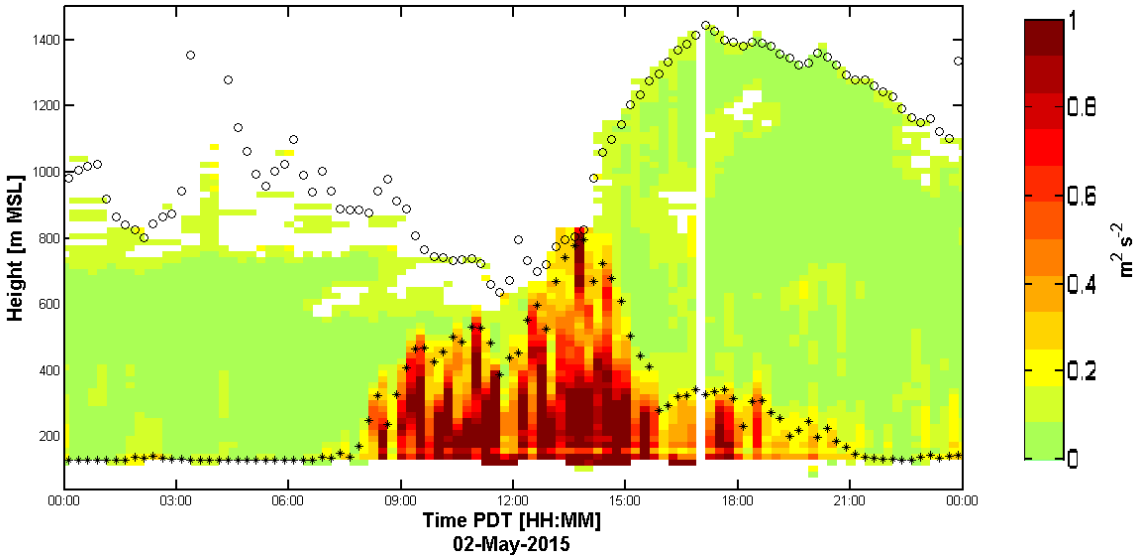

Figure 24: Vertical velocity variance derived from Doppler LiDAR at SJSU on 02 May 2015. Warmer (red and orange) colors represent a more positive vertical velocity variance (m^2 s^{-2}), while cooler (green) colors are lower values. The estimated CBL height is illustrated by an asterisk (*), and aerosol depth is illustrated by an open circle (o). The x-axis represents local time (PDT), and the y-axis depicts the height (m MSL).

Comparing the CBL on 02 May to that of 01 May, the initial growth of the estimated CBL height occurs one hour apart. Figure 25 indicates stronger low-level winds in the early pre-dawn hours on 01 May, potentially inhibiting the initial CBL growth. This strong low-level wind core from the south on 01 May 2015 (Figure 16 and 17) is more apparent than on 02 May 2015 (Figure 25 and 26). This drainage flow is due to the down-valley flow from Gilroy toward the San Francisco Bay. Its absence on 02 May is speculated to cause the initial CBL height growth to occur at approximately 0730 PDT as opposed to 0830 PDT the previous day. One likely cause of the earlier start of CBL height growth on 02 May 2015 may be the presence of clouds aloft. This would reduce the impact that *H* would have in the post-dawn hours. However, it is noted that neither the SK in Figure 27 nor the backscatter in Figure 28 suggest the presence of low-level

stratocumulus; although clouds above approximately 1000-1500 m MSL are not detectable by the Doppler LiDAR due to range limitations.

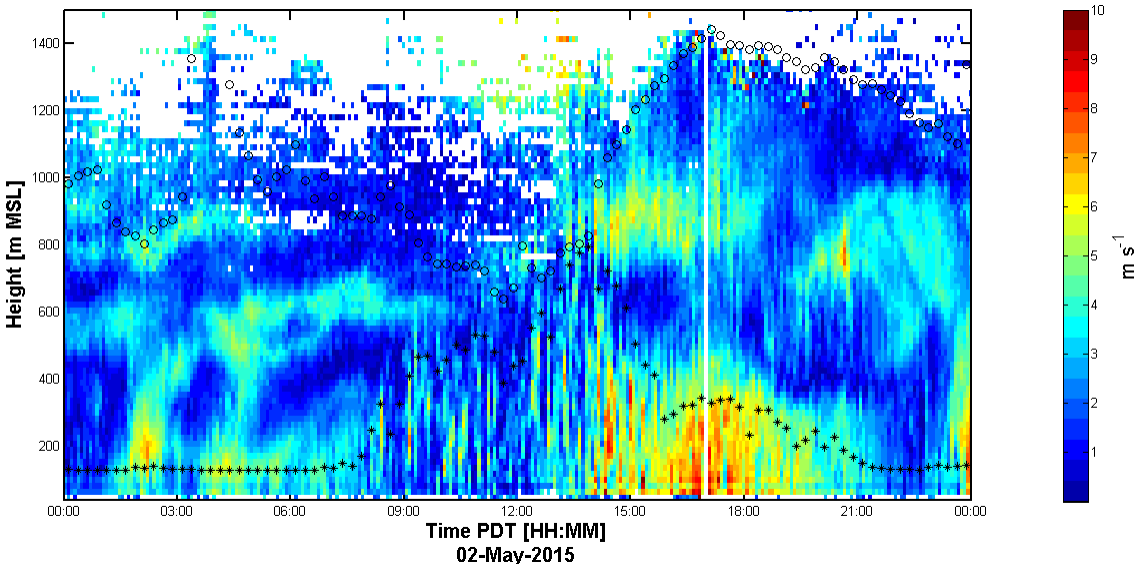

Figure 25: Wind speed profile using Doppler LiDAR at SJSU on 02 May 2015. The estimated CBL height is illustrated by an asterisk (*), and the estimated aerosol depth is illustrated by an open circle (o). The x-axis represents local time (PDT), with y-axis depicting the height (m MSL).

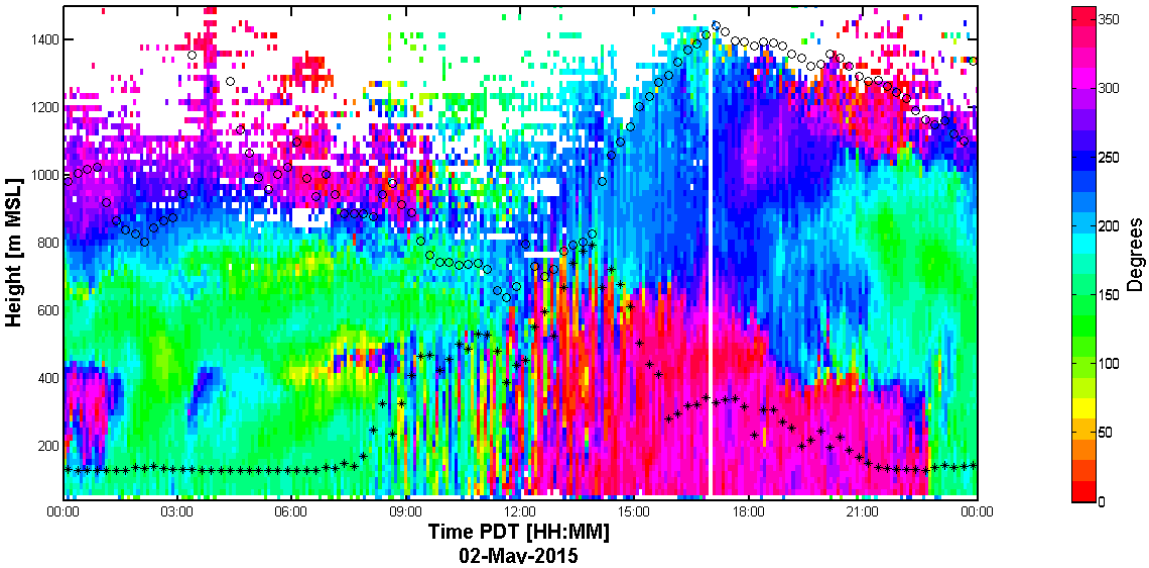

Figure 26: Wind direction profile using Doppler LiDAR at SJSU on 02 May 2015. The estimated CBL height is illustrated by an asterisk (*), and the estimated aerosol depth is illustrated by an open circle (o). The x-axis represents local time (PDT), with y-axis depicting the height (m MSL).

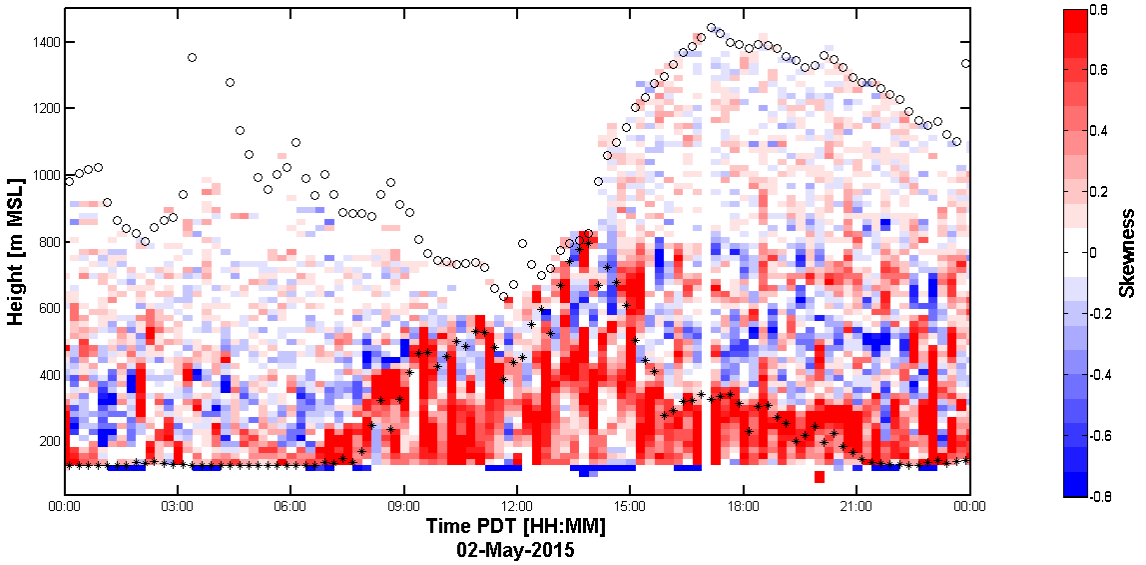

Figure 27: Vertical velocity skewness profile using Doppler LiDAR at SJSU on 02 May 2015. Warmer (red) colors represent positive vertical velocity skewness, while cooler (blue) colors represent negative vertical velocity skewness. The estimated CBL height is illustrated by an asterisk (*), and aerosol depth is illustrated by an open circle (o). The x-axis represents local time (PDT), and the y-axis depicts the height (m MSL).

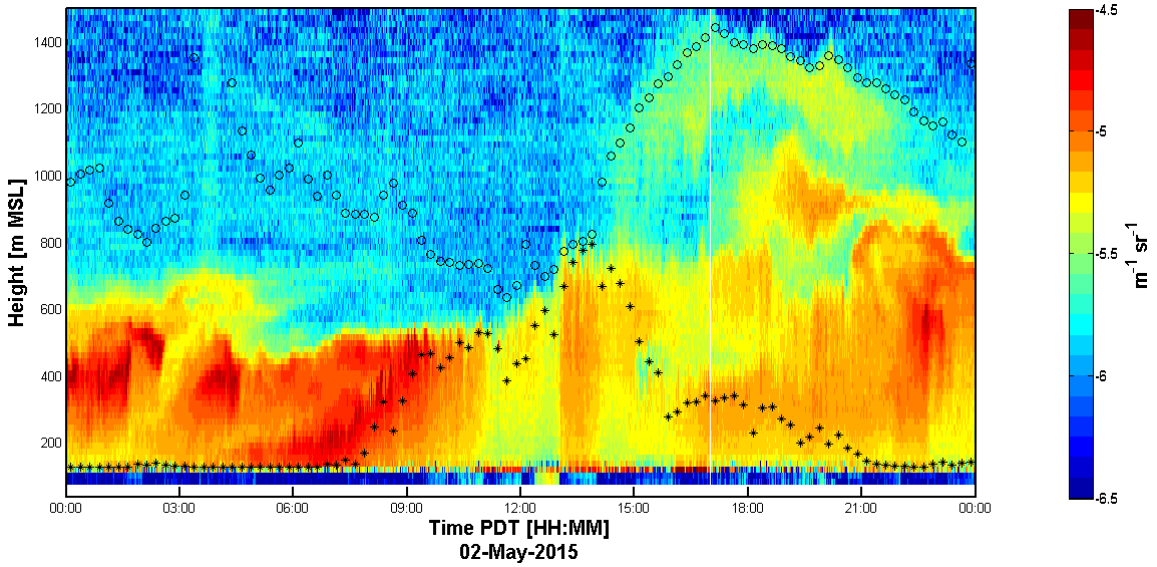

Figure 28: Attenuated backscatter profile using Doppler LiDAR at SJSU on 02 May 2015. Warmer (red and orange) colors represent a more positive backscatter (m^{-1} sr^{-1}), while cooler (blue) colors represent more negative backscatter. The estimated CBL height is illustrated by an asterisk (*), and aerosol depth is illustrated by open circles (o). The x-axis represents local time (PDT), with y-axis depicting the height (m MSL).

The sea breeze FROPA is as evident on 02 May 2015 as it was the previous day due to the directional wind shift to northwesterly at nearly the same time. It is estimated that the sea breeze FROPA occurred 20 min later than the previous day, at approximately 1330 PDT. The dew point temperature at SJS01 (Figure 8) sees an increase of 3 °C between 1200 PDT and 1500 PDT, compared to an increase of 3.3 °C in 2.5 h during a similar time frame on the previous day's sea breeze FROPA.

The near-surface winds up to 800 m MSL in the morning on 02 May 2015 are southeasterly as depicted in Figure 26. This represents a light down-valley or offshore wind, with the greatest low-level winds at 200 m MSL reaching 5-7 m s^{-1} before sunrise as seen in Figure 25. In comparison to 01 May 2015 (in Figure 16), the horizontal wind velocities are approximately 2-3 m s^{-1} lower. The winds below 800 m MSL within the CBL remain light (below 5 m s^{-1}) but become more variable from 0800 PDT to 1200 PDT. Following the peak CBL height at approximately 1330 PDT, the winds are stronger (up to approximately 8 m s^{-1}) and have shifted to northwesterly, ushering in the MBL. The collapse of the CBL height from 1330 PDT to 1600 PDT and the increase in dew point temperature both suggest the presence of a sea breeze FROPA accompanied with the onset of differential cold air advection suppressing the convective mixing from the surface.

Following the collapse of the peak CBL height, the residual turbulence decreases due to the intrusion of the MBL near the surface. This region of reduced turbulence from 1400 PDT to the end of the period, at heights up to well over 1000 m MSL represents the RL. It is noted that there is a decoupling in the RL in Figure 28. It is speculated that this

is due to the vertically propagating AD, similar to that on 30 April 2015 as seen in Figure 11 and again in Figure12. However, the evidence in Figure 24 is not as conclusive with the σ_w^2 aloft to guarantee a rising AD.

The region aloft, near 800 m MSL following 1330 PDT to the end of the day, sees a decrease in vertical velocity and σ_w^2. The SK in the RL is more neutral than that within the CBL, indicating that the turbulence is becoming more isotropic and characteristic of a layer of decaying turbulence.

This period summarizes another example of a clear CBL with an afternoon sea breeze FROPA on 02 May 2015 in San Jose. It is noted that the maximum temperature of 23 °C represents a third consecutive day of cooling, indicating the onshore push of the WCTT The onshore push of the WCTT encourages the effects of the continued general sea breeze circulation pattern and the sea breeze FROPA in the PBL in San Jose. The estimated CBL height growth initiated approximately one hour earlier than the CBL on 01 May 2015. It is speculated that this time differential is due to the absence of the stronger drainage flow that is evident on 01 May 2015 in Figure 16 and 17, but not on 02 May 2015 in Figure 25 and 26. It is also noted that a decoupling of the RL occurs following the peak CBL height.

4) Clear CBL With Afternoon Sea Breeze Frontal Passage – 03 May 2015

This period on 03 May 2015 exemplifies a mostly-clear CBL with an afternoon sea breeze FROPA and a MBL influence in San Jose. The growth of the CBL height begins early on 03 May 2015, as illustrated in Figure 29. Shortly after sunrise at about 0700 PDT, the CBL grows rapidly to a daily maximum over 1000 m MSL at about 1330 PDT.

The CBL height recedes approximately 200 m before stabilizing near 900 m MSL until a rapid collapse at 1600 PDT. The CBL height is near surface levels by 2100 PDT, or about one hour after sunset.

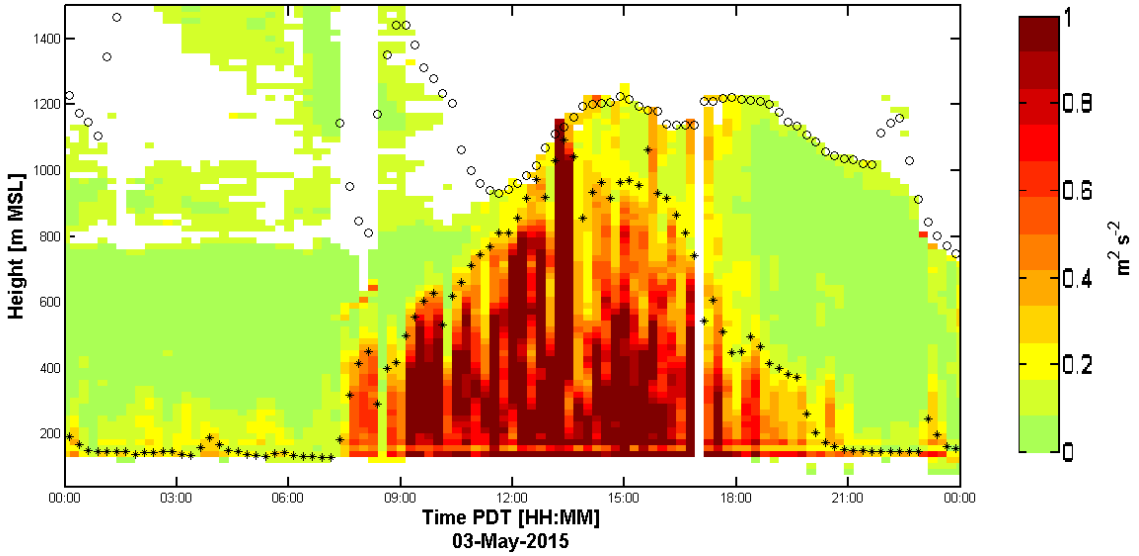

Figure 29: Vertical velocity variance derived from Doppler LiDAR at SJSU on 03 May 2015. Warmer (red and orange) colors represent a more positive vertical velocity variance (m^2 s^{-2}), while cooler (green) colors are lower values. The estimated CBL height is illustrated by an asterisk (*), and aerosol depth is illustrated by an open circle (o). The x-axis represents local time (PDT), and the y-axis depicts the height (m MSL).

The weather conditions are very similar to the previous day, creating another sea breeze FROPA event. In Figure 30, the wind direction is uniform from the southeast at all levels to 800 m MSL in the morning, indicative of a well-organized sea breeze circulation pattern. Figure 31 depicts high winds slightly above 200 m MSL with values of 8 m s^{-1}.

During the growing phase of the CBL height, the winds begin to veer westward, with a decrease in wind speed near the surface to approximately 1-4 m s^{-1}. Following the peak CBL height around 1330 PDT, winds below 600 m MSL are mostly northwesterly. Another wind speed core lies near the surface to heights of 400 m MSL; although not as

persistent as the morning land breeze (or drainage flow), this sea breeze does produce northwesterly winds of 5-7 m s^{-1} (Figure 30 and 31).

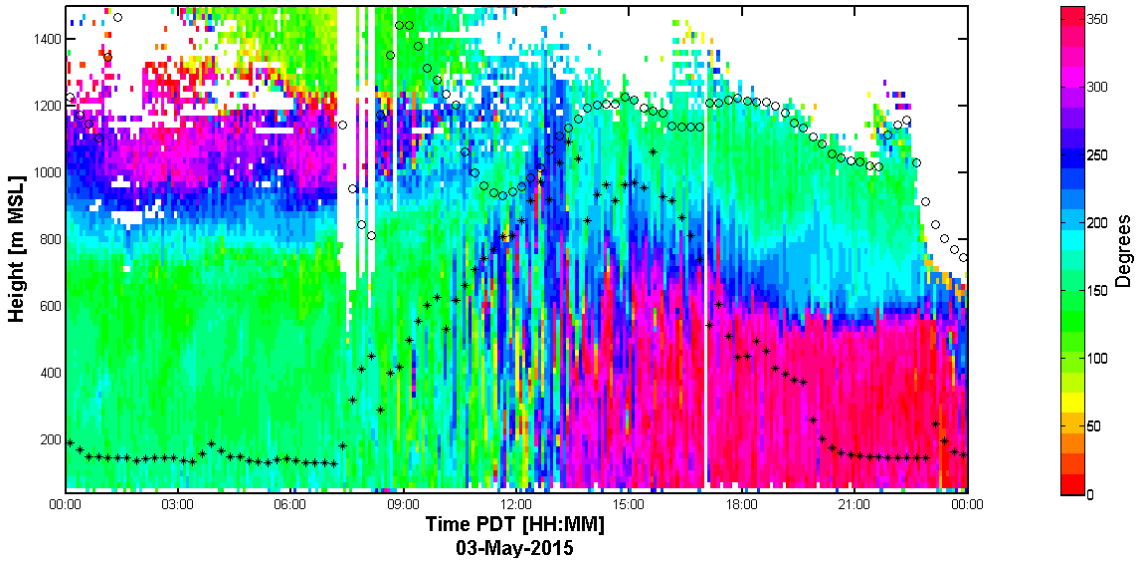

Figure 30: Wind direction profile using Doppler LiDAR at SJSU on 03 May 2015. The estimated CBL height is illustrated by an asterisk (*), and the estimated aerosol depth is illustrated by an open circle (o). The x-axis represents local time (PDT), with y-axis depicting the height (m MSL).

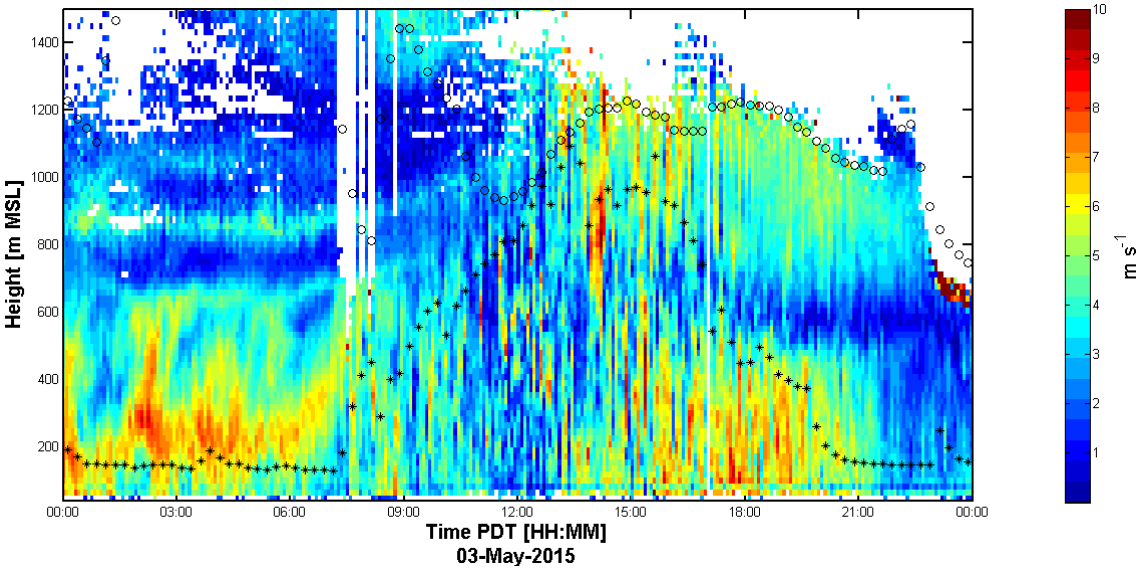

Figure 31: Wind speed profile using Doppler LiDAR at SJSU on 03 May 2015. The estimated CBL height is illustrated by an asterisk (*), and the estimated aerosol depth is illustrated by an open circle (o). The x-axis represents local time (PDT), with y-axis depicting the height (m MSL).

This onshore push from the northwest is opposing the preceding drainage flow from the southeast. During this phase of the wind reversal near the surface, the land breeze is lifted above the sea breeze during the latter half of the day. The AD is lifted to at least 1200 m MSL following the peak of the CBL height. Vertically propagating residual thermals are evident in Figure 29 and 32 immediately following the peak CBL height. This region above the decaying CBL height is the RL.

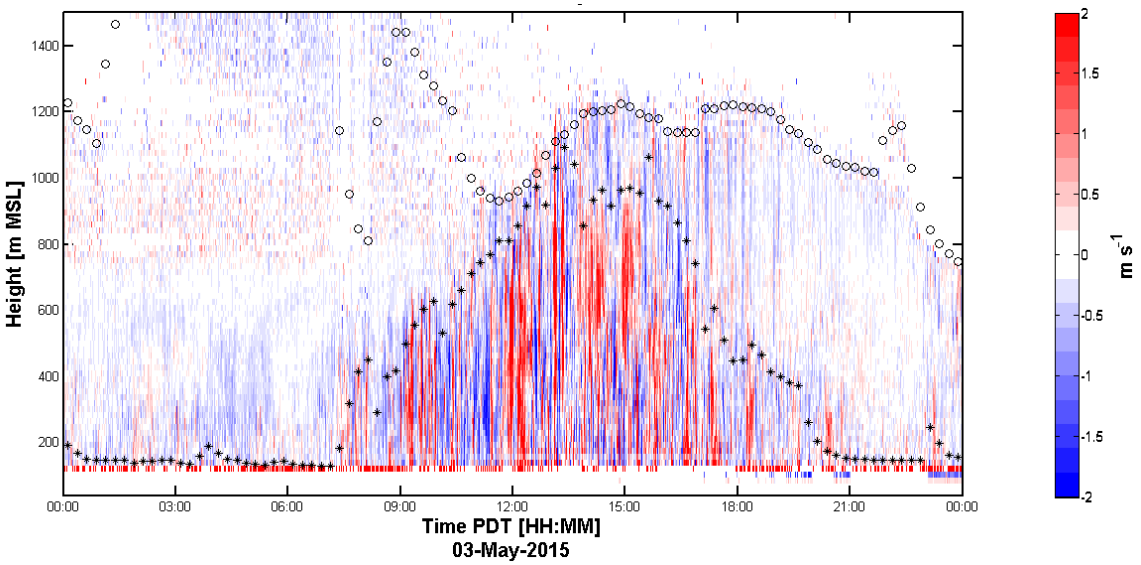

Figure 32: Vertical velocity profile using Doppler LiDAR at SJSU on 03 May 2015. Warmer (red) colors represent positive (upward) vertical velocity (m s^{-1}), while cooler (blue) colors represent negative (downward) vertical velocity. The estimated CBL height is illustrated by an asterisk (*), and aerosol depth is depicted by an open circle (o). The x-axis represents local time (PDT), with y-axis depicting the height (m MSL).

These events represent an example of a diurnal land-sea breeze circulation. As seen at station SJS01 in Figure 8, at about 1310 PDT (near peak CBL height growth), the maximum temperature of 22.9 °C is reached. After 50 min, the temperature drops to 19.8 °C in connection with the sea breeze FROPA. Another key indicator of the arrival of the sea breeze is the increase in dew point temperature. Between 1240-1425 PDT, the dew

point temperature increases from 9.1 °C to 10.9 °C. The 200 m reduction in CBL height, immediately following the peak around 1330 PDT, is a result of the sea breeze FROPA.

The SK is especially positive during the CBL height growth stage in Figure 33 between 0730 PDT and 1300 PDT. Another region of positive SK is near the surface as the CBL height collapses from 1800 PDT to the end of the period and from the surface to approximately 400 m MSL. Unique features are found in the attenuated backscatter in Figure 34 which occur near the end of the period. The greater (darker red) values nearest to -4.5 m^{-1} sr^{-1} suggest a cloud layer, or cloud base, being formed above the Doppler LiDAR at 500-800 m MSL beginning at approximately 2230 PDT and continues into the next period on 04 May 2015. A smaller period of low clouds is present in Figure 34 between 300-600 m MSL and lasts about three hours starting near 0600 PDT.

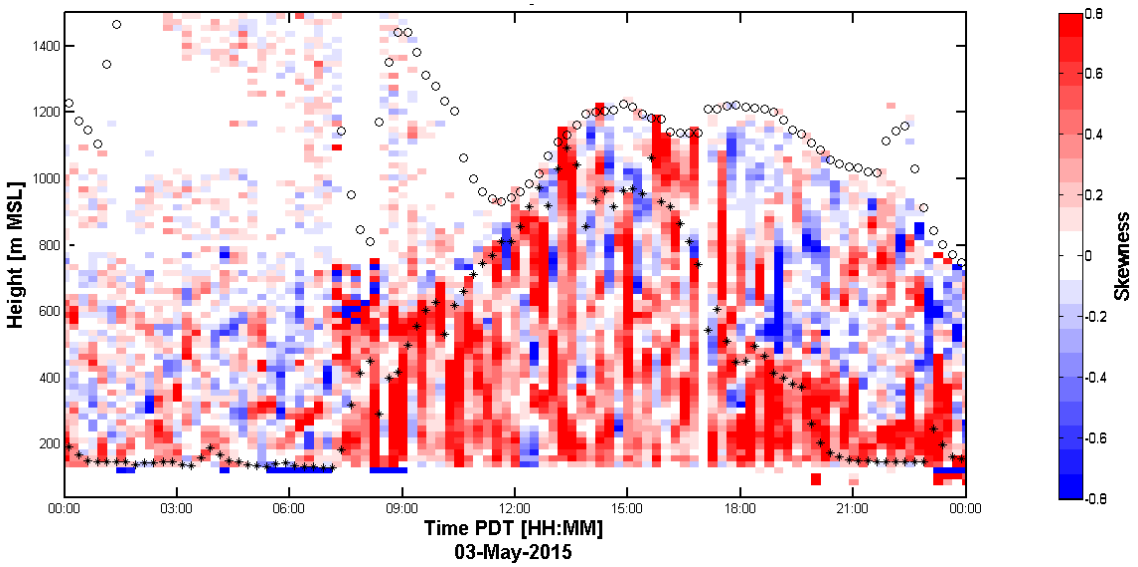

Figure 33: Vertical velocity skewness profile using Doppler LiDAR at SJSU on 03 May 2015. Warmer (red) colors represent positive vertical velocity skewness, while cooler (blue) colors represent negative vertical velocity skewness. The estimated CBL height is illustrated by an asterisk (*), and aerosol depth is illustrated by an open circle (o). The x-axis represents local time (PDT), and the y-axis depicts the height (m MSL).

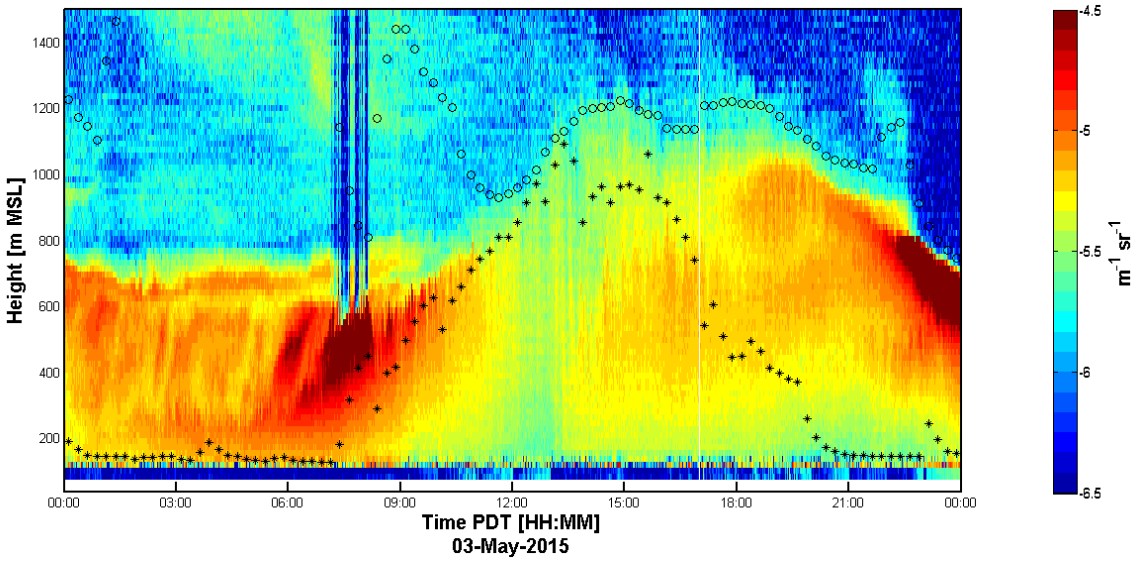

Figure 34: Attenuated backscatter profile using Doppler LiDAR at SJSU on 03 May 2015. Warmer (red and orange) colors represent a more positive backscatter (m^{-1} sr^{-1}), while cooler (blue) colors represent more negative backscatter. The estimated CBL height is illustrated by an asterisk (*), and aerosol depth is illustrated by open circles (o). The x-axis represents local time (PDT), with y-axis depicting the height (m MSL).

In conclusion for the period on 03 May 2015, evidence from the applied methods suggest a mostly-clear CBL with a sea breeze FROPA in San Jose. Only a brief period of low clouds occurs in the morning near sunrise. Typical sea breeze circulation patterns are portrayed in Figure 30. The sea breeze FROPA occurs at approximately 1300 PDT when considering the increase of dew point temperature begins near 1240 PDT and the wind direction shifts from southeasterly to northwesterly at approximately 1330 PDT. In the three examples of a clear CBL with a sea breeze FROPA, it is noted that they occur within 30 min of the same time in the afternoon. The gradual cooling trend continues following the absence of the WCTT. As indicated by the SJS01 station, the maximum temperature for 03 May 2015 was approximately 22.9 °C at 1330 PDT. The unique feature in this period is the attenuating backscatter return in Figure 34 illustrating the beginning of a cloud layer or cloud base.

5) Nocturnal Stratocumulus-Topped Boundary Layer – 04 May 2015

This period on 04 May 2015 identifies a nocturnal stratocumulus-topped PBL that transitions to a clear CBL during the day in San Jose. Nearly two hours after sunrise at about 0800 PDT, CBL height growth is initiated. Peak CBL height is estimated to be approximately 800 m MSL at 1500 PDT. A complete collapse and decay of the CBL height is estimated to take place by 2100 PDT, approximately one hour after sunset.

The unique feature of this period is situated in the attenuated backscatter returns portrayed in Figure 35. The morning hours of 04 May 2015, between 0000 and about 1145 PDT, consist of a low-elevation cloud base located between an estimated 400-800 m MSL. Due to the high optical thickness of the stratocumulus, the Doppler LiDAR returns are not capable of penetrating to levels above 700-900 m MSL. It appears that the height of the cloud base in Figure 35 is increasing as convective mixing protrudes upward, assisting in the morning burning off of the clouds.

Station SJS01 in Figure 8 illustrates the influence that the cloud layer has on nocturnal surface weather observations. The temperature holds steady near 12-13 °C through the period until 1010 PDT. As the morning clouds decay by about noon, the Doppler LiDAR's backscatter increase (indicating a cloudless layer at those levels). Between 0000 and 1030 PDT the RH in Figure 8 is steady between 70-79%, and then drops briefly to 55% at 1230 PDT, also suggesting an approximate time of stratocumulus burn off. The temperature is suppressed and limited to 17.9 °C. This is due to the marine influence of the nocturnal stratocumulus-topped PBL.

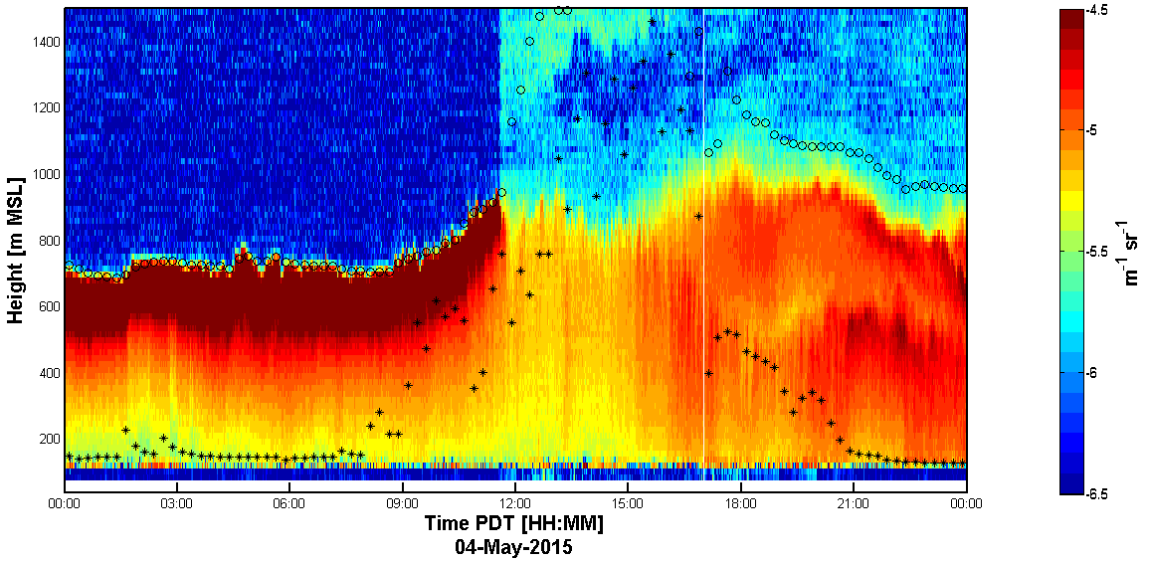

Figure 35: Attenuated backscatter profile using Doppler LiDAR at SJSU on 04 May 2015. Warmer (red and orange) colors represent a more positive backscatter (m^{-1} sr^{-1}), while cooler (blue) colors represent more negative backscatter. The estimated CBL height is illustrated by an asterisk (*), and aerosol depth is illustrated by open circles (o). The x-axis represents local time (PDT), with y-axis depicting the height (m MSL).

The SK profile in Figure 36 illustrates the impact of the low cloud layer in the morning. Between 400 and 700 m MSL and before approximately 0900 PDT, the nocturnal stratocumulus-topped PBL is dominated by negatively skewed vertical motions, indicative of cloud top radiative cooling. This is an example of the "top down" source of turbulent motions, where turbulence is greatest aloft yet decreases toward the earth's surface. Essentially, TKE is being transported toward the surface in this area of negative SK.

The source of turbulence is also evident in Figure 37. Between approximately 0000 PDT and 0900 PDT, there is a maxima of σ_w^2 depicting the vertical motions that are due to the nocturnal stratocumulus-topped PBL; this variance is not illustrated to this degree in the previous days during the evening hours. At approximately 0600 PDT, the area

beneath the stratocumulus-topped PBL is elevated to approximately 500-700 m MSL while the σ_w^2 profile in Figure 37 exhibits returns up to 0.6 m^2 s^{-2}. It is also observed that narrow bands of downward (negative) vertical velocity dominate in Figure 38 at this same time and space.

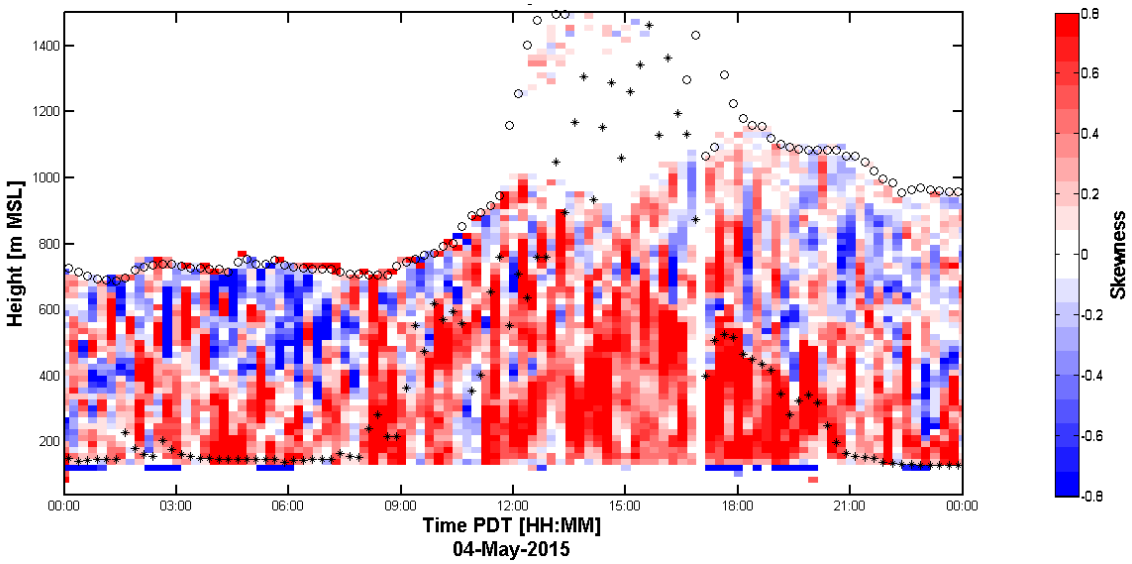

Figure 36: Vertical velocity skewness profile using Doppler LiDAR at SJSU on 04 May 2015. Warmer (red) colors represent positive vertical velocity skewness, while cooler (blue) colors represent negative vertical velocity skewness. The estimated CBL height is illustrated by an asterisk (*), and aerosol depth is illustrated by an open circle (o). The x-axis represents local time (PDT), and the y-axis depicts the height (m MSL).

It is evident that positive SK in Figure 36 is most abundant within the daytime CBL, similar to the preceding days. Following the collapse of the CBL height at about 1700 PDT, the RL is indicated by the reduction of vertical velocity close to 0 m s^{-1} near 500 to 800 m MSL in Figure 38, a neutralization of the SK in Figure 36, and a reduction in σ_w^2 near 0 m^2 s^{-2} in Figure 37. The RL continues through the end of the period with an estimated height of the AD determined to be around 1000 m MSL.

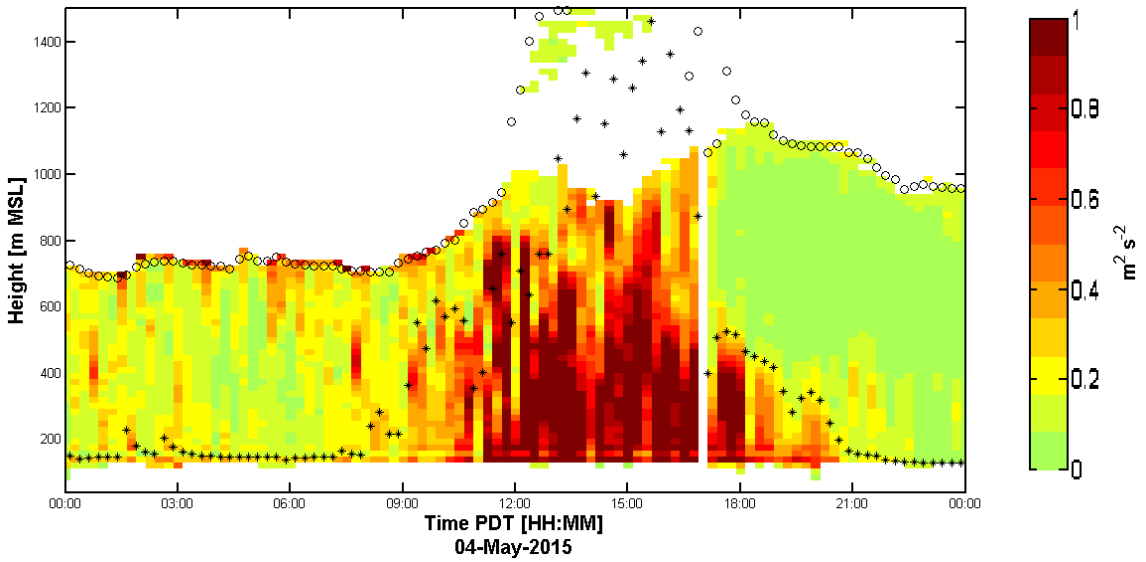

Figure 37: Vertical velocity variance derived from Doppler LiDAR at SJSU on 04 May 2015. Warmer (red and orange) colors represent a more positive vertical velocity variance (m^2 s^{-2}), while cooler (green) colors are lower values. The estimated CBL height is illustrated by an asterisk (*), and aerosol depth is illustrated by an open circle (o). The x-axis represents local time (PDT), and the y-axis depicts the height (m MSL).

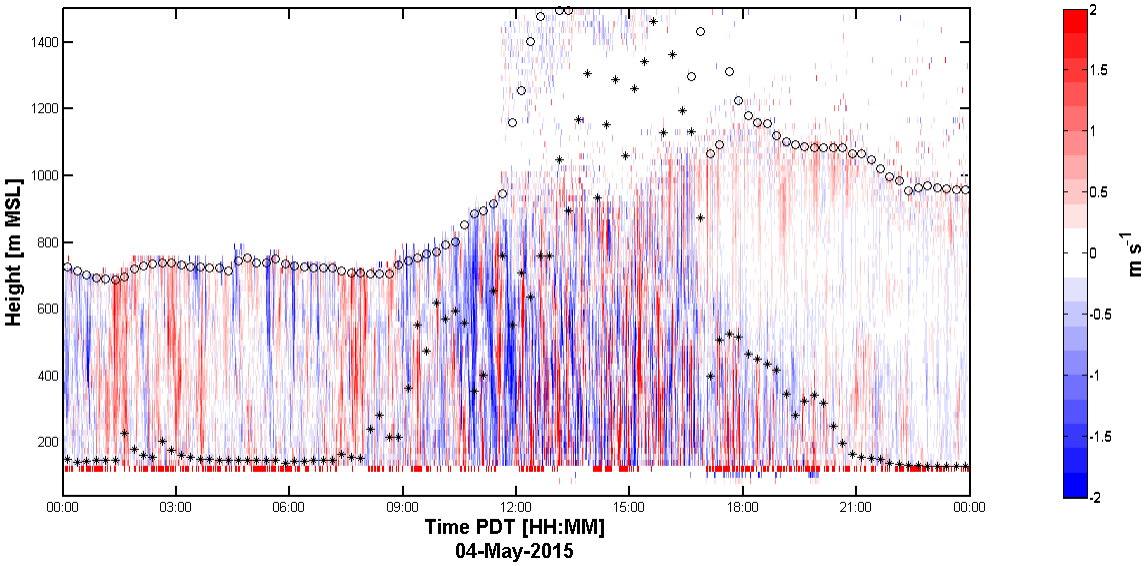

Figure 38: Vertical velocity profile using Doppler LiDAR at SJSU on 04 May 2015. Warmer (red) colors represent positive (upward) vertical velocity (m s^{-1}), while cooler (blue) colors represent negative (downward) vertical velocity. The estimated CBL height is illustrated by an asterisk (*), and aerosol depth is depicted by an open circle (o). The x-axis represents local time (PDT), with y-axis depicting the height (m MSL).

The wind characteristics differ slightly from what was seen on preceding days. In Figures 39 and 40, the southeast winds representing the drainage flow from 0300 PDT to 0800 PDT are light. This drainage flow is brief and exhibits wind speeds below 4 m s^{-1} throughout the vertical profile, suggesting a weaker circulation. The northwest winds begin at approximately 1200 PDT, in a region between the surface and approximately 600 m MSL, and persist through the end of the period. This flow, influenced by the sea breeze circulation pattern, consists of a core up to about 500 m MSL from the surface and is most prevalent between 1600 PDT and 2000 PDT. The highest wind speeds within the core are about 8 m s^{-1}.

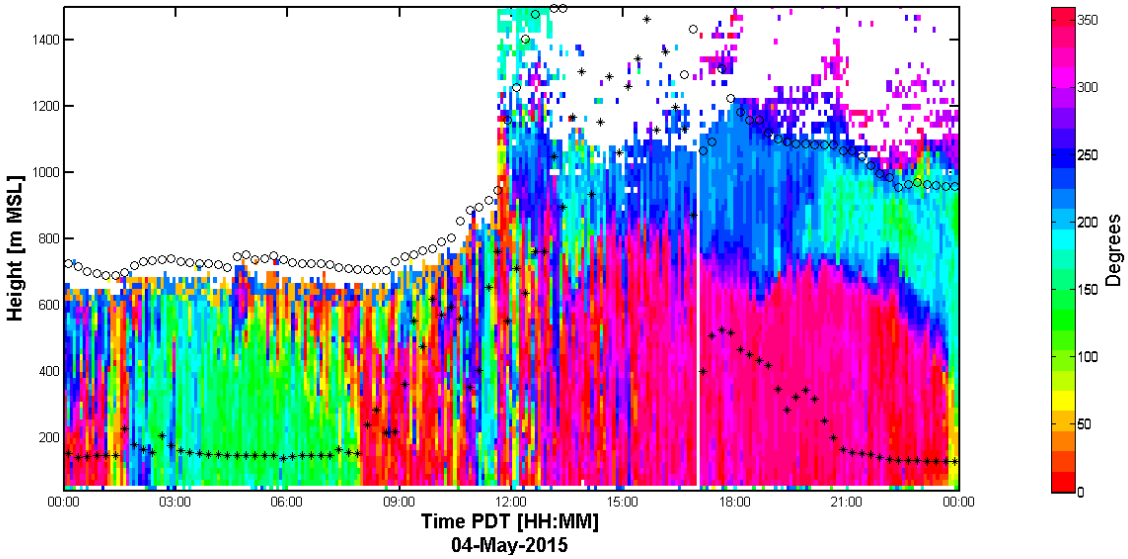

Figure 39: Wind direction profile using Doppler LiDAR at SJSU on 04 May 2015. The estimated CBL height is illustrated by an asterisk (*), and the estimated aerosol depth is illustrated by an open circle (o). The x-axis represents local time (PDT), with y-axis depicting the height (m MSL).

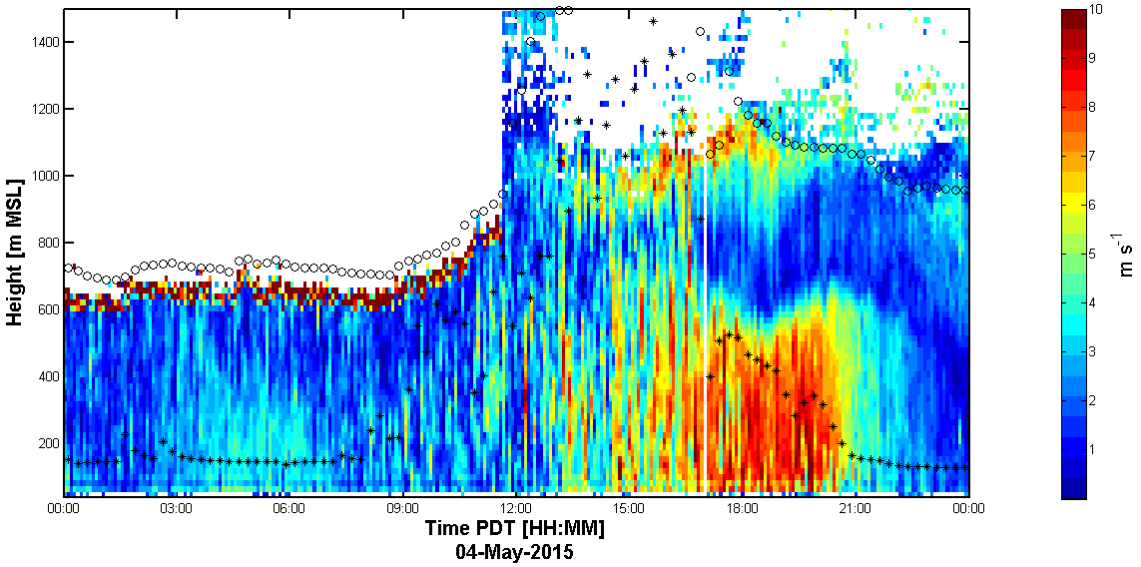

Figure 40: Wind speed profile using Doppler LiDAR at SJSU on 04 May 2015. The estimated CBL height is illustrated by an asterisk (*), and the estimated aerosol depth is illustrated by an open circle (o). The x-axis represents local time (PDT), with y-axis depicting the height (m MSL).

This period on 04 May 2015 is dominated by a MBL. With suppressed temperatures, reduced surface-based turbulence (negative SK aloft in the morning hours), and weaker surface-level winds, there lacks any noticeable sea breeze FROPA due to the fact that a boundary of air masses is not attainable. A nocturnal stratocumulus-topped PBL defines this period and set the tone for the distinguishable characteristics that were evident using the Doppler LiDAR methods.

6) Summary

The case study for 30 April 2015 through 04 May 2015 was selected because of the distinct examples of evolving PBL types that are presented. The methods of σ_w^2 for estimating the CBL height and SK for distinguishing the source of turbulent flows functioned appropriately in this case study. These various PBL conditions were identified using the vertical staring Doppler LiDAR in concert with the SJS01 station, Geopotential

height field, and OAK atmospheric soundings to analyze three common types of PBLs in San Jose: clear CBL with minimal marine influence, clear CBL with sea breeze FROPA, and nocturnal stratocumulus-topped PBL.

5. Climatology of the CBL Height in San Jose

This chapterdiscusses the San Jose, California climatology of the PBL, namely the CBL during the daytime, during a period between June 2013 and August 2015. During this approximately two year period, the SJSU Doppler LiDAR remained on the rooftop as it collected data via the vertical stare scan mode. Composite monthly mean CBL heights during this period were calculated from Doppler LiDAR observations. The results are analyzed and discussed.

The monthly mean CBL heights were obtained in the same manner as was used in the case study presented in the previous chapter. The method of the σ_w^2 profile with the threshold of 0.1 m^2 s^{-2} was used to identify the estimated CBL height through the period of approximately two years of June 2013 through August 2015. While the Doppler LiDAR was actively collecting data most of the time, there are periods of missing data. Some of the missing data is due to the Doppler LiDAR switching to overheating mode, being utilized for other research, or other reasons causing data to be omitted from the climatology.

The remaining observations allowed 393 viable days to be applied to the monthly mean maximum CBL height climatology, as seen in Figure 41. A seasonal trend is noted throughout the period where the microclimate of San Jose is manifested, particularly in

the summer with a decrease in CBL height. The climatology of the CBL height can be identified in three distinct, extended periods in San Jose: spring, summer, and winter.

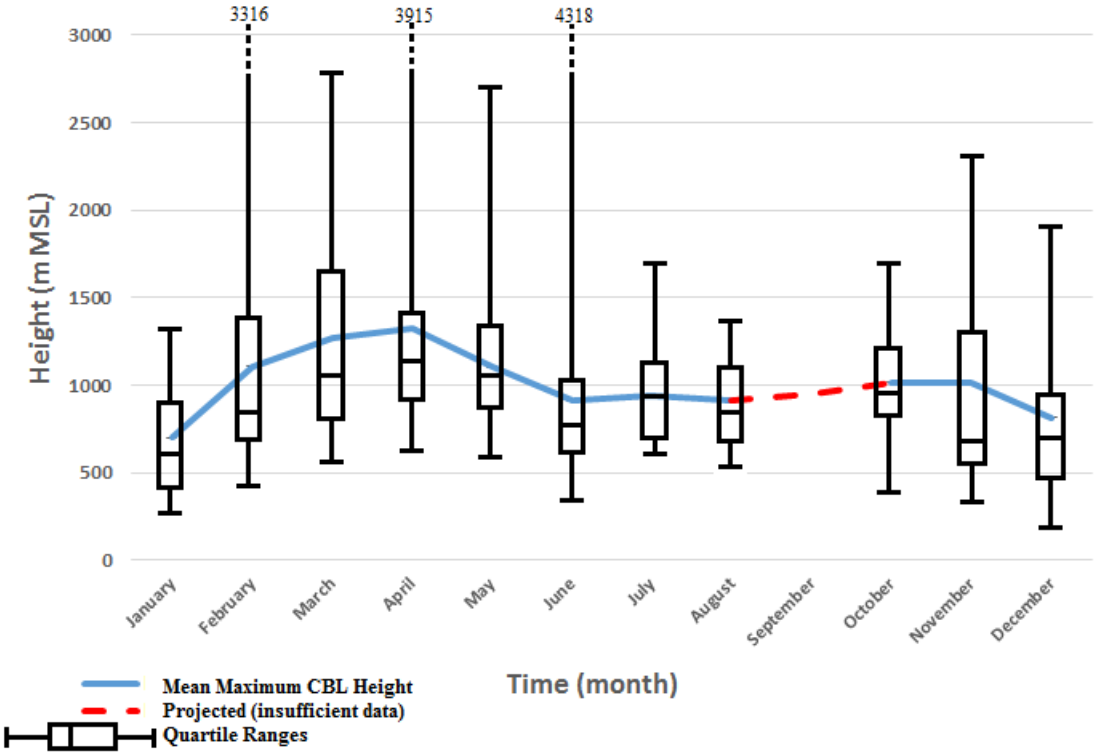

Figure 41: Monthly maximum CBL height (black quartile ranges) climatology at SJS01 2013-2015. Mean maximum CBL height (solid blue line) and projected CBL height (hashed red line). The x-axis is time (month). The y-axis is height (m MSL).

The CBL height is greatest in the months of February through May (representing the seasonal transition period), highlighting the spring season. Figure 41 shows that the mean maximum CBL height exceeds 1100 m MSL during these months. As the solar angle increases (resulting in greater *H*), turbulent mixing is enhanced. This turbulent energy exchange is transported vertically, causing an increase in the height of the ML. It is hypothesized that the higher CBL heights in spring are due to the lack of a recurring MBL (whereas the MBL is more common in the summertime).

In the summer months of June, July, August (and the subsequent two months of September and October), suppression of the maximum CBL height is apparent. Figure 41 depicts the mean CBL heights during this period from 908-1017 m MSL. From July to October, monthly maximum CBL heights are suppressed to below 1750 m MSL, whereas earlier months of the year see heights exceeding 2500 m MSL and even a few days near 4000 m MSL in April and June. During the months of June through October, the monthly mean maximum CBL heights are in closer alignment with the median heights. San Jose is commonly impacted by the MBL during this period.

As illustrated in the case study in Chapter 4, Figures 35 through 40 exhibit a nocturnal stratocumulus-topped PBL due to a presence of the MBL in early May. Another example of the common summertime occurrence is illustrated in the attenuated backscatter profile on 15 July 2015 in Figure 42. Higher attenuated backscatter is evident between approximately 400-800 m MSL from the beginning of the period through about 0730 PDT. This suggests a low-level cloud layer in the PBL such as stratocumulus. Note the suppressed CBL heights in this example. Although the breakup of the low cloud layer occurs at approximately 0730 PDT, the influence of this MBL restricts CBL height growth to below 800 m MSL for much of the period, only briefly exceeding approximately 875 m MSL between 1430 PDT and 1445 PDT. This restricted CBL height and suppression is likely associated with the low-level cloud layer (or stratocumulus) that is indicative of a marine layer. There is a stabilization of the CBL due to differential temperature advection as colder air advects near the surface, inhibiting vertical mixing. This suppression of land-based surface heating is identified by a top

down source of turbulence as opposed to the typical bottom up profile that is common in the daytime in the absence of a MBL.

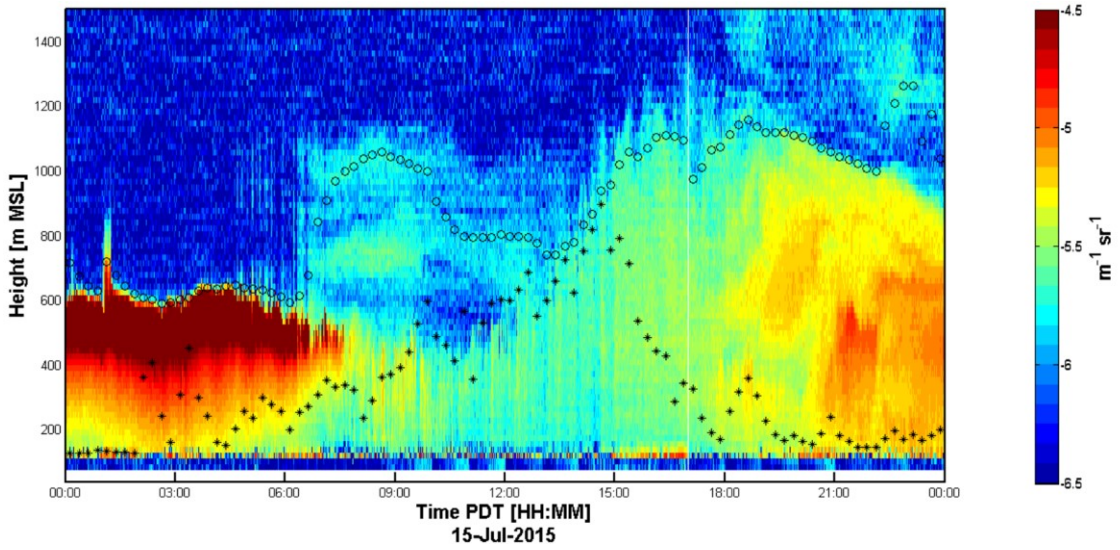

Figure 42: Attenuated backscatter profile using Doppler LiDAR at SJSU on 15 July 2015. Warmer (red and orange) colors represent a more positive backscatter (m^{-1} sr^{-1}), while cooler (blue) colors represent more negative backscatter. The estimated CBL height is illustrated by an asterisk (*), and aerosol depth is illustrated by open circles (o). The x-axis represents local time (PDT), with y-axis depicting the height (m MSL).

Further evidence of this summer time MBL in San Jose is illustrated in the Doppler LiDAR's σ_w^2 profile in Figure 43 and the SK profile in Figure 44. It is noted in Figure 43 that between 0200 PDT and approximately 0430 PDT there is a region of increased turbulence near the surface to about 600 m MSL. It is speculated that this is due to the presence of the nocturnal stratocumulus layer as seen in the attenuating backscatter in Figure 42. Negative SK is identified in Figure 44 in this same region, and continues along the top of the estimated CBL height through the period.

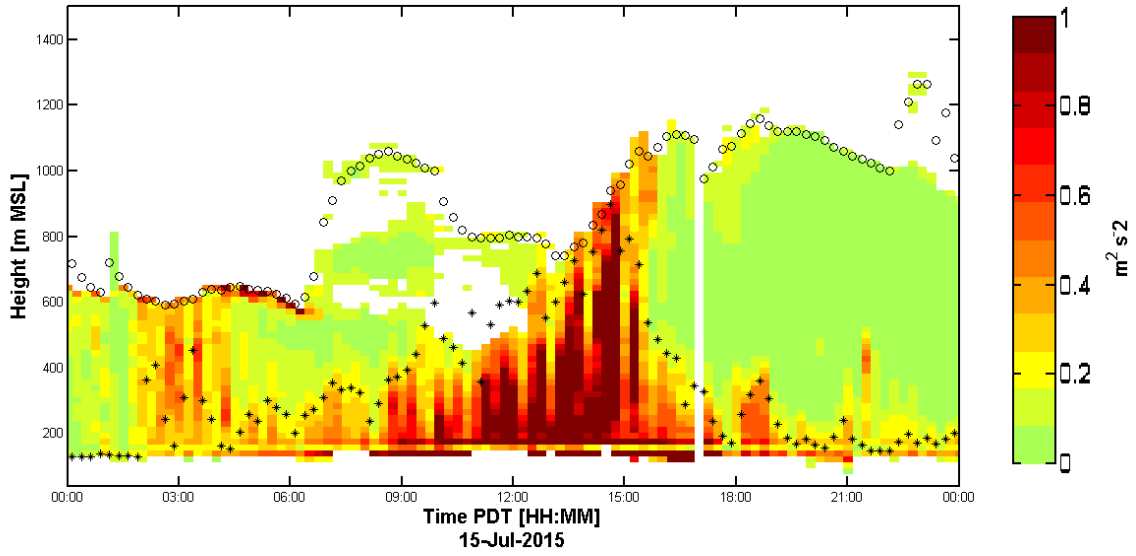

Figure 43: Vertical velocity variance derived from Doppler LiDAR at SJSU on 15 July 2015. Warmer (red and orange) colors represent a more positive vertical velocity variance (m^2 s^{-2}), while cooler (green) colors are lower values. The estimated CBL height is illustrated by an asterisk (*), and aerosol depth is illustrated by an open circle (o). The x-axis represents local time (PDT), and the y-axis depicts the height (m MSL).

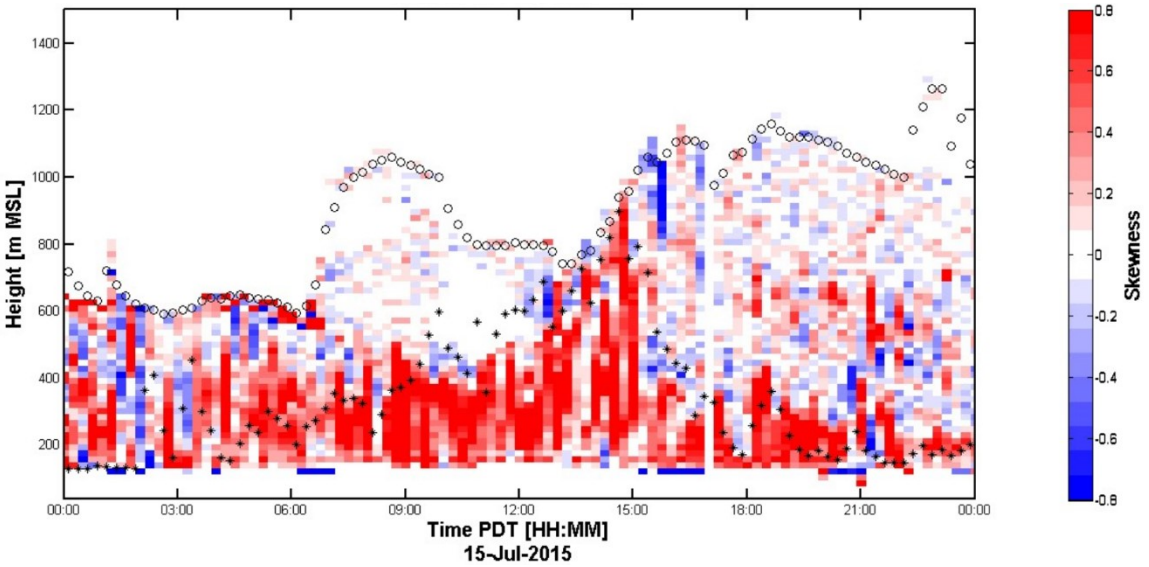

Figure 44: Vertical velocity skewness profile using Doppler LiDAR at SJSU on 15 July 2015. Warmer (red) colors represent positive vertical velocity skewness, while cooler (blue) colors represent negative vertical velocity skewness. The estimated CBL height is illustrated by an asterisk (*), and aerosol depth is illustrated by an open circle (o). The x-axis represents local time (PDT), and the y-axis depicts the height (m MSL).

The monthly mean CBL height trend in Figure 41 depicts a transition to lower levels in winter (in the months of November, December, and January). Low insolation at the surface due to the annually-low solar angle is a driving factor in the lowest mean CBL heights of the year in San Jose. CBL heights are frequently below 1000 m MSL, with December seeing a mean of 813 m MSL, and January at 699 m MSL. A sample of the lower winter season CBL height is evident in the vertical velocity profile on 04 January 2014 (see Figure 45). The CBL height is suppressed for a majority of the period. Only between approximately 1200 PDT and 1700 PDT is there CBL height growth. Shortly after 1600 PDT, the CBL height only briefly exceeds 400 m MSL. During this peak CBL height time, the vertical velocity illustrates only a few narrow updrafts within the CBL. The AD varies between approximately 500-1000 m MSL through the period.

The climatology of the CBL height in San Jose varies by season. The trends in Figure 41 reiterate the impact that the seasons have on the PBL in the area. It is speculated that the spring months bring the highest CBL heights due to two theories: first, an increase in *H* during the spring months, and second, factors related to synoptically-influenced weather phenomena. During the spring months the transition from winter to summer sees an increase in *H*, while avoiding the CBL-suppressing onshore push of the MBL that is more common in the summer. Regarding common examples of synoptic-scale occurrences, FROPAs encourage mixing and provide aided growth of the CBL height, as identified by the determination methods used in this paper.

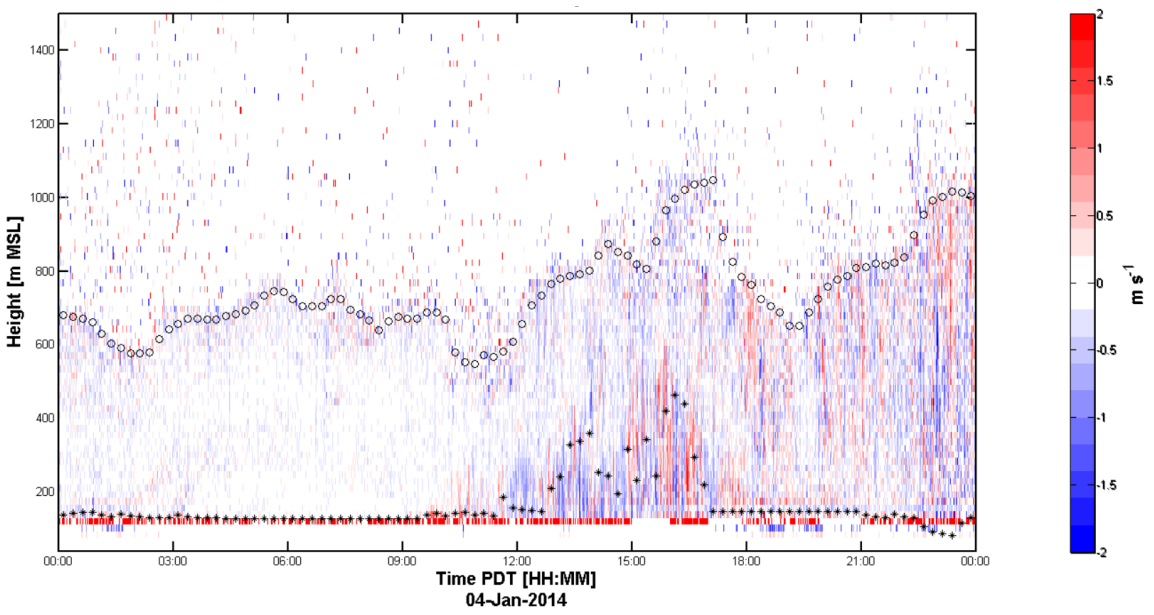

Figure 45: Vertical velocity profile using Doppler LiDAR at SJSU on 04 January 2015. Warmer (red) colors represent positive (upward) vertical velocity (m s^{-1}), while cooler (blue) colors represent negative (downward) vertical velocity. The estimated CBL height is illustrated by an asterisk (*), and aerosol depth is depicted by an open circle (o). The x-axis represents local time (PDT), with y-axis depicting the height (m MSL).

The summer months provide the most favorable conditions for an intruding MBL to impact the PBL in San Jose, therefore reducing the maximum CBL heights during the period. According to Bridger et al. (1993), when the semi-permanent Pacific high establishes itself, it is common to see stratocumulus- and stratus-topped inversion layers in the summer. This MBL is a result of the sharp gradient of the high pressure subsidence creating warm, dry air aloft in contrast to the cool, moist marine air near the surface (Bridger et al. 1993). As the climatological high weakens near the end of the summer months, and this temperature and moisture gradient is reduced, the impact of the MBL on the CBL heights is lessened.

Transitioning into the months of November, December, and January, the cause of even lower CBL heights is due to the lower solar angle, the decrease in daylight. The sun is the source of CBL growth. It can be concluded that the primary driver of suppressed CBL height growth during these winter months is the reduction of *H*.

6. Discussion and Conclusions

We have examined the anatomy and basic mechanics of the PBL, discussed applications of PBL meteorology, and identified common types of the PBL in San Jose. The CBL, often analogous to the daytime PBL, is the portion of the PBL affected by the friction of the earth's surface and responds to surface forcing within a time scale of one hour or less (Stull 1988). The CBL is initiated during the daytime, is buoyancy driven, and is driven by surface sensible and latent heat fluxes. As illustrated in Figure 1, the ML is this region of the PBL during the daytime that consists of turbulent eddies and vertical motions; these ultimately determine whether the CBL is growing or decaying. The EZ is a region of atmospheric transfer between the ML and the FA. The entrainment of pollutants, or other gases, can mix through the EZ to be transported into the FA, emphasizing one of the applications of PBL meteorology to air quality and pollution management. Wind energy corporations consider turbulence for production efficiency and also to protect the integrity of the wind turbines. The importance of PBL meteorology was also discussed for the travel industry and the general public.

A main purpose of this paper was to apply two statistical measures of the PBL structure in a case study of the PBL in San Jose, California using Doppler LiDAR data. The use of other parameters from the Doppler LiDAR data was supplementary in the

study, namely, vertical velocity (from which the two methods are based), attenuated backscatter, wind direction, and wind speed profiles. The OAK atmospheric soundings and 925 hPa geopotential height data were also used in the case study to assist in the analysis of a WCTT to illustrate the impacts of one example of a synoptic scale phenomenon on the CBL and other surface weather observations.

During the five-day case study, we analyzed the PBL in San Jose with the σ_w^2 and SK methods. These profiles of the PBL were produced to determine the estimated CBL height, locate sources of turbulence, and identify the different types of the PBL. The σ_w^2 method includes empirically setting a variance threshold in the dataset to determine the estimated CBL height (Tucker et al. 2009). In this paper, we used 0.1 m^2 s^{-2} to define the upper bound of turbulent mixing, where regions with σ_w^2 greater than this threshold were considered well-mixed and part of the ML, or CBL. The SK method by Hogan et al. (2009) helped differentiate between types of the PBL and identified the source and location of TKE. PBL types that were cloudless or cumulus-topped (representing fair weather conditions) contained a positive SK profile. Positive SK suggested that turbulence was "bottom up" and driven by land-based heating of the ground (Hogan et al. 2009), or *H*. In the case study, the PBL was positively skewed during the clear CBL with minimal marine influence. During the sea breeze FROPA in the case study, the SK profile remained mostly positive within the CBL; however, in the afternoon hours following the sea breeze FROPA, negative SK was common near the EZ. Finally, the nocturnal stratocumulus-topped PBL in the case study depicted the most negatively skewed profile. While positive SK was identified, negative SK throughout the upper-third

of the ML was evident when clouds were overhead. This indicated the presence of a cloud-topped PBL and "top down" turbulence profile (TKE being transported toward the surface rather than solely from a surface-based profile). The σ_w^2 and SK profile methods, with an analysis of other parameters, were successfully applied in San Jose.

The use of the σ_w^2 method to determine the height of the CBL proved worthy of a brief climatology study. The San Jose Doppler LiDAR dataset runs through much of 2013 through 2015. The climatology of monthly mean maximum CBL heights were produced in Figure 41. It was observed that maximum CBL heights were greatest in March and April, with adjacent months of February and May, all grouped into the "spring" season. The monthly mean maximum CBL heights for the spring season ranged from approximately 1104-1320 m MSL. For the warm season, comprising June through October, the monthly mean maximum CBL heights were suppressed, with a range from approximately 908-1017 m MSL. The winter season experienced the lowest monthly mean maximum CBL height. November, December, and January saw a range from approximately 699-1109 m MSL. It was speculated that the spring season's highest values were due to a balance of the increase of insolation, or *H,* and the less frequent MBL to suppress the CBL height. Recall that the recurring MBL in the warm season is estimated to be a cause in the slight suppression in CBL heights during that period. The winter experienced the lowest solar angle, greatly inhibiting vertical mixing and CBL height growth.

Future work would be beneficial as a supplement to the findings in this study. While the case study clearly identifies and validates previous methods for boundary layer

analyses in a coastal urban environment, closer analysis of the Doppler LiDAR data with a focus on distinguishing the common CBL regimes would improve the identification of their occurrences and frequencies. This focus on the climatology of the Doppler LiDAR data could aid in confirming the aforementioned questions of when, why, and how the different types of CBL occur in San Jose, California. This future work will also be more appealing as a longer dataset becomes available through continued data collection over the next several years.

REFERENCES

Angevine, W., A. White, and S. K. Avery, 1994: Boundary-layer depth and entrainment zone characterization with a boundary-layer profiler. **68**.

Bianco, L., I. Djalalova, C. King, and J. Wilczak, 2011: Diurnal evolution and annual variability of boundary-layer height and its correlation to other meteorological variables in California's Central Valley. *Bound.-Layer Meteorol.,* **140**, 491-511.

Bougeault, P., J. André, 1986: On the stability of the third-order turbulence closure for the modeling of the stratocumulus-topped boundary layer. *J. Atmos. Sci.,* **43**, 1574-1581.

Brewer, M., C. Mass, B. Potter, 2012: The West Coast Thermal Trough: Climatology and Synoptic Evolution. *Mon. Weather Rev.,* **140**, 3820-3843.

Bridger, A. F., W. C. Brick, and P. F. Lester, 1993: The structure of the marine inversion layer off the central California coast: Mesoscale conditions. *Mon. Weather Rev.,* **121**, 335-351.

Cleugh, H., C. Grimmond, 2001: Modelling regional scale surface energy exchanges and CBL growth in a heterogeneous, urban-rural landscape. *Bound.-Layer Meteorol.,* **98**, 1-31.

Cohn, S.A., W. M. Angevine, 2000: Boundary layer height and entrainment zone thickness measured by lidars and wind-profiling radars. *J. Appl. Meteorol.,* **39**, 1233-1247.

Eichinger, W., H. Holder, R. Knight, J. Nichols, D. Cooper, L. Hipps, W. Kustas, and J. Prueger, 2005: Lidar measurements of boundary layer evolution to determine sensible heat fluxes. *J. Hydrometeorol.*, **6**, 840-853.

Engelmann, R., U. Wandinger, A. Ansmann, D. Müller, E. Žeromskis, D. Althausen, and B. Wehner, 2008: Lidar observations of the vertical aerosol flux in the planetary boundary layer. *J. Atmos. Ocean. Technol.,* **25**, 1296-1306.

Eresmaa, N., J. Härkönen, S. M. Joffre, D. M. Schultz, A. Karppinen, and J. Kukkonen, 2012: A three-step method for estimating the mixing height using ceilometer data from the Helsinki Testbed. Journal of Applied Meteorology and Climatology, **51**, 2172-2187.

Fischer, M.L. et al., 2016: A Survey of Methane Emissions from the California Natural Gas System. Report # 500-12-027 (in press).

Frehlich, R., 2008: Doppler lidar measurements of winds and turbulence in the boundary layer. *Proc. IOP Conference Series: Earth and Environmental Science,* IOP Publishing, 012017.

Frehlich, R., Y. Meillier, and M. L. Jensen, 2008: Measurements of boundary layer profiles with in situ sensors and Doppler lidar. *J. Atmos. Ocean. Technol.,* **25**, 1328-1340, doi:10.1175/2007JTECHA963.1.

Hogan, R. J., A. L. M. Grant, A. J. Illingworth, G. N. Pearson, and E. J. O'Connor, 2009: Vertical velocity variance and skewness in clear and cloud-topped boundary layers as revealed by Doppler lidar. *Q. J. R. Meteorol. Soc.,* **135**, 635-643, doi:10.1002/qj.413.

Holton, J.R.: 1972, *An Introduction to Dynamic Meteorology*. Academic Press, 90-91, 319.

Hooper, W. P., E. W. Eloranta, 1986: Lidar measurements of wind in the planetary boundary layer: the method, accuracy and results from joint measurements with radiosonde and kytoon. *Journal of climate and applied meteorology,* **25**, 990-1001.

Horel et al., Department of Atmospheric Sciences, University of Utah. MesoWest, accessed 20 May 2016. [Available online at: http://mesowest.utah.edu/cgi-bin/droman/download_api2.cgi?stn=SJS01&hour1=00&min1=50&timetype=LOCAL&unit=0&graph=0]

Kaimal, J.C., J. J. Finnigan, 1994: Atmospheric boundary layer flows: their structure and measurement.

Ketterer, C., P. Zieger, N. Bukowiecki, M. C. Coen, O. Maier, D. Ruffieux, and E. Weingartner, 2014: Investigation of the planetary boundary layer in the Swiss Alps using remote sensing and in situ measurements. *Bound.-Layer Meteorol*., **151**, 317-334.

Kossmann, M., R. Vögtlin, U. Corsmeier, B. Vogel, F. Fiedler, H. Binder, N. Kalthoff, and F. Beyrich, 1998: Aspects of the convective boundary layer structure over complex terrain. *Atmos. Environ.,* **32**, 1323-1348.

Leung, L. R., W. I. Gustafson, 2005: Potential regional climate change and implications to US air quality. Geophys. Res. Lett., **32**.

McElroy, J. L., T. B. Smith, 1991: Lidar descriptions of mixing-layer thickness characteristics in a complex terrain/coastal environment. *J. Appl. Meteorol*., **30**, 585-597.

Moeng, C., R. Rotunno, 1990: Vertical-velocity skewness in the buoyancy-driven boundary layer. J. Atmos. Sci., **47**, 1149-1162.

Moyer, K. A., G. S. Young, 1991: Observations of vertical velocity skewness within the marine stratocumulus-topped boundary layer. *J. Atmos. Sci*., **48**, 403-410.

Nicholls, S., M. A. LeMone, 1980: The fair weather boundary layer in GATE: The relationship of subcloud fluxes and structure to the distribution and enhancement of cumulus clouds. *J. Atmos. Sci*., **37**, 2051-2067.

Reuten, C., D. Steyn, K. Strawbridge, and P. Bovis, 2005: Observations of the relation between upslope flows and the convective boundary layer in steep terrain. *Bound.-Layer Meteorol.,* **116**, 37-61, doi:10.1007/s10546-004-7299-7.

Rhodes, M. E., J. K. Lundquist, 2013: The effect of wind-turbine wakes on summertime US Midwest atmospheric wind profiles as observed with ground-based doppler lidar. Bound.-Layer Meteorol., **149**, 85-103.

Steyn, D., M. Baldi, and R. Hoff, 1999: The detection of mixed layer depth and entrainment zone thickness from lidar backscatter profiles. *J. Atmos. Ocean. Technol*., **16**, 953-959, doi:10.1175/15200426(1999)016<0953:TDOMLD>2.0.CO;2.

Stull, R.B., 1988: *An Introduction to Boundary Layer Meteorology*. Kluwer Academic Publishers, 666.

Tucker, S. C., C. J. Senff, A. M. Weickmann, W. Brewer, R. M. Banta, S. P. Sandberg, D. C. Law, and R. Hardesty, 2009: Doppler Lidar Estimation of Mixing Height Using Turbulence, Shear, and Aerosol Profiles. *J. Atmos. Ocean. Technol.,* **26**, 673-688, doi: http://dx.doi.org/10.1175/2008JTECHA1157.1.

Wang, J., R. L. Bras, 1998: A new method for estimation of sensible heat flux from air temperature. *Water Resour. Res.,* **34**, 2281-2288.

Wang, Z., X. Cao, L. Zhang, J. Notholt, B. Zhou, R. Liu, and B. Zhang, 2012: Lidar measurement of planetary boundary layer height and comparison with microwave profiling radiometer observation. *Atmospheric Measurement Techniques,* **5**, 1965-1972, doi:10.5194/amt-5-1965-2012.